Near Earth Object (NEO) Mitigation Options Using Exploration Technologies

Robert B. Adams[1], Jonathan W. Campbell[2], Randall C. Hopkins[3] and W. Scott Smith[4]
National Aeronautics and Space Administration, Marshall Space Flight Center, MSFC, AL, 35812

William Arnold[5]
Jacob Sverdrup, Huntsville, AL 35812

Mike Baysinger[6] and Tracie Crane[7]
Qualis Corporation, Huntsville, AL 35805

Pete Capizzo[8] and Steven Sutherlin[9]
Raytheon Corporation, Huntsville, AL 35806

John Dankanich[10] and Gordon Woodcock[11]
Gray Research Inc., Huntsville, AL 35806

George Edlin[12] and Johnny Rushing[13]
Alpha Technology, Inc., Huntsville, AL 35801

Leo Fabisinski[14], David Jones[15], Steve McKamey[16] and Scott Thomas[17]
International Space Systems, Inc., Huntsville, AL 35816

Claudio Maccone[18]
Member of the International Academy of Astronautics, Torino, Turin, Italy

Greg Matloff[19]
New York City College of Technology, Brooklyn, NY, 11201

John Remo[20]
Harvard University, Cambridge, MA 02138

[1] Advanced Propulsion Technologist, EI63/Advanced Concepts, Senior Member AIAA.
[2] Space Systems Engineer/Scientist, EV13/Space Environments, Associate Fellow AIAA.
[3] Aerospace Engineer (Vehicle Design and Mission Analysis), EI63/Advanced Concepts.
[4] Optical Physics, VP63/Optics.
[5] Senior Principal Engineer, VP63/Optics.
[6] Design Engineer,EI63/Advanced Concepts, 5000 Bradford Drive, Suite 3B.
[7] Engineer, EI63/Advanced Concepts, 5000 Bradford Drive, Suite 3B.
[8] Electrical and Avionics System Engineer, EI63/Advanced Concepts, 401 Jan Davis Drive.
[9] Principal Multi-Discipline Engineer, ER23/Spacecraft Propulsion Systems, 401 Jan Davis Drive.
[10] Aerospace Engineer, 655 Discovery Drive, Suite 300, Member AIAA.
[11] Senior Engineer, 655 Discovery Drive, Suite 300, Associate Fellow AIAA.
[12] Chief Scientist, Nuclear and Directed Energy Concepts, 3322 South Memorial Parkway, Suite 630.
[13] Physicist, Nuclear and Directed Energy Concepts, 3322 South Memorial Parkway, Suite 630.
[14] Director of Software Engineering, EI63/Advanced Concepts, 555 Sparkman Drive Suite 608.
[15] Mechanical Engineer, EI63/Advanced Concepts, 555 Sparkman Drive Suite 608.
[16] Areospace Engineer, EI63/Advanced Concepts, 555 Sparkman Drive Suite 608.
[17] Mechanical Engineer, EI63/Advanced Concepts, 555 Sparkman Drive Suite 608, Member AIAA.
[18] Retired Scientist, Via Martorelli 43.
[19] Assistant Professor, Physics Department, 300 Jay Street.
[20] Professor, Department of Astronomy, Department of Earth and Planetary Science.

[Abstract] This work documents the advancements in MSFC threat modeling and mitigation technology research completed since our last major publication in this field. Most of the work enclosed here are refinements of our work documented in NASA TP-2004-213089. Very long development times from start of funding (10-20 years) can be expected for any mitigation system which suggests that delaying consideration of mitigation technologies could leave the Earth in an unprotected state for a significant period of time. Fortunately there is the potential for strong synergy between architecture requirements for some threat mitigators and crewed deep space exploration. Thus planetary defense has the potential to be integrated into the current U.S. space exploration effort. The number of possible options available for protection against the NEO threat was too numerous for them to all be addressed within the study; instead, a representative selection were modeled and evaluated. A summary of the major lessons learned during this study is presented, as are recommendations for future work.

Nomenclature

$M_{asteroid}$ = mass of the asteroid to be deflected

$\rho_{asteroid}$ = density of the asteroid

$D_{asteroid}$ = diameter of the asteroid assumed to be spherical to simplify things

m_{bullet} = mass of the bullet or bullet, i.e. the missile whose kinetic energy will deflect the asteroid by kinetic impact. In this study, the bullet's mass is assumed to be 1500 kg.

v_{bullet} = bullet's speed at the instant of final crash against the asteroid, i.e. deflection

E_{bullet} = kinetic energy of the bullet at the instant of crash against the asteroid

v_{Max_bullet} = Maximum bullet speed at the crash still capable of avoiding fragmentation. That is, bullet's speeds below this value are acceptable since they cause craterization of the asteroid only. Speeds above this value are not acceptable since they would fragment the asteroid, thus complicating the issue further.

I. Introduction

In 2004 NASA embarked on a new vision to explore space[1]. The architecture that resulted includes a human rated launch vehicle and a heavy lift cargo vehicle. Both vehicles are derived from shuttle technology. The crewed launcher, the Ares I, is slated to be complete by 2014. The heavy lift vehicle is called the Ares V and is currently scheduled to be completed by 2020. The vision defines the objectives of returning humans to the moon in 2020 in preparation for future crewed exploration of Mars and other destinations.

In 2004 NASA published a review[2] of mitigation technologies for defending the planet from Near Earth Objects (NEO's). This review was completed at the George C. Marshall Space Flight Center and several of the authors of this paper were contributors. Although the results of the 2004 technical paper were preliminary, they suggest that mitigation methods would benefit greatly from the existence of a heavy lift launch vehicle. Another result of the 2004 study was the need for advanced propulsion technologies. Many of these technologies are also applicable to crewed deep space exploration.

Clearly there is the potential for substantial synergy between the objective of crewed deep space exploration and planetary defense. Both missions will require delivery of considerable payloads with propulsion systems that produce substantial ΔV. Additionally both missions will experience similar environments in interplanetary space in the inner solar system where Earth and Mars both orbit. Finally, the Vision for Space Exploration requires preparation for crewed exploration of Mars and other destinations. Crewed visitation of an NEO would be an excellent candidate for an intermediate mission between returning to the moon and the first landing on Mars; with a degree of difficulty in operations, ΔV and space environment between the two missions above.

What is also clear is that in the current political environment and the numerous issues faced by the United States, there is precious little extraneous funding for new missions like planetary defense. NASA has its hands full completing the near term task of returning to the moon while maintaining agency

priorities in earth and space science, education, legacy infrastructure, etc. The direction of the study described herein is to consider what can be done in the realm of planetary defense using the Vision for Space Exploration architecture and minimal new technology development. Perhaps in the future, planetary defense will rise high enough in the pantheon of the country's priorities to expect advanced propulsion research to be funded in the process of designing a more capable planetary defense system.

II. Approach, Groundrules and Assumptions

Many of the groundrules and assumptions for the study are derived from the dual requirements that the vehicles for the Vision for Space Exploration architecture are available and that minimal new funding is available to support development of a new planetary defense architecture. From this it is easily concluded that only near term technologies should be considered. Times to bring vehicles from concept to operation can easily range from 5-10 years. Therefore, it is not unreasonable to assume that a planetary defense system, requiring minimal technology development, could be operational by the time the Ares V is brought on line, i.e. 2020.

To implement the above assumptions the study considered technologies at TRL 5 or better.

Current knowledge of the NEO population is limited. Current knowledge of NEO's does not include a strong understanding of the densities or internal structure of most asteroids and comets. Whether the NEO in question has a dust cloud or satellites is not usually known. Current detection systems cannot determine orbital parameters, size or geometry with a high degree of accuracy. This study assumes that there is not a substantial increase in the capability of current detection systems or the understanding of the physical parameters of NEO's.

III. Concept of Operations

Both the Ares I and Ares V vehicles are used in the operational concept for this study. At some point after 2020 current or future detection systems determine that a NEO has a substantial probability of striking the Earth in the near future. When the probability exceeds a threshold determined by the appropriate governing body (i.e. Congress or the President for a NASA developed system) the operational plan for NEO threat mitigation will be put into action.

The first step will be to launch an observer satellite on the Ares I to yield the required information on the NEO. This observer satellite will either rendezvous or fly-by the NEO. Observer operations, to be described in a later section, will be designed to yield highly accurate information on the internal structure and possible composition of the NEO, as well as its geometry, rotation, orbital elements and the potential for orbiting dust, debris or small satellites.

With this information, the probability of impact as well as the consequences of impact can be estimated to a much higher level of accuracy. If the results suggest further action is needed to protect the populace (again based on guidelines ratified by the appropriate governing body) then one of the interceptor options will be launched.

Which interceptor is launched is determined by the results from the observer satellite. The most capable interceptor will be launched based on time before impact, size and composition of the NEO, etc. The interceptor will be launched on an Ares V launch vehicle. Based on the interceptor option, the interceptor will either collide with or rendezvous with the NEO. Each option has a different method of interacting with the NEO to mitigate the threat posed. The section on interceptor options will go into further detail the operational plan for each of the options. It should be noted that if possible the observer satellite will rendezvous with the NEO. Not only will this offer additional time to characterize the NEO, it will give an additional asset to observe the NEO while it is being affected by the interceptor, should the interceptor be needed.

IV. Ares Launch Vehicle Description

The designs for the Ares I and Ares V are currently in the state of development. Other documents define the design and capabilities of these vehicles in detail. This section describes the Ares I and Ares V from the state of their design when this study was completed.

The Ares I vehicle is shown in Figure 1. The stack is comprised of a first stage that is a Reusable Solid Rocket Motor (RSRM) modified from the current Shuttle Transportation System (STS) to add an additional fifth motor segment. The second stage is a new design utilizing liquid oxygen (Lox) and liquid hydrogen

(LH2) propellants and a modified version of the J-2 engine used on the second and third stages of the Saturn V launch vehicle. The relevant parameters and performance of the Ares I are listed in Table 1.

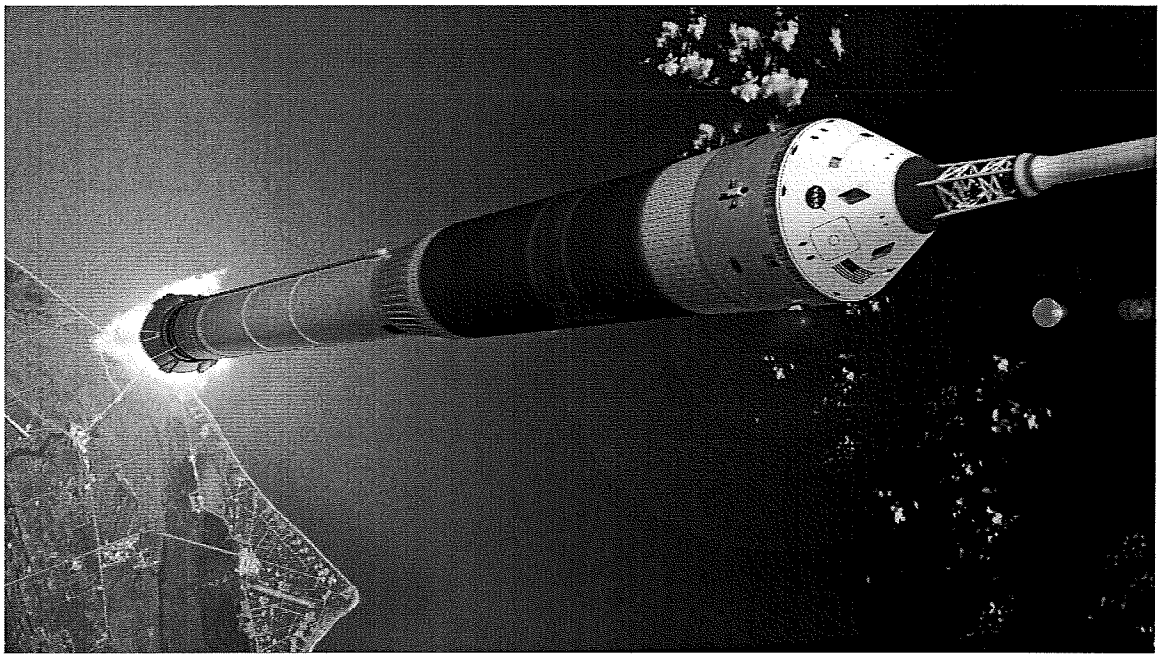

Figure 1: Ares I Depicted Launching From Kennedy Space Center

The Ares V vehicle is shown in Figure 2. The vehicle design is based on the STS stack. The orbiter is removed from the stack. The external tank is extended and the payload is placed on top of it for the new Ares V design. The Ares V specifications and performance is also listed in Table 1.

Table 1: Performance and specifications for the Ares I and Ares V

Target Orbit/C3	Inclination	Ares I Payload	Ares V Payload
-30 x 100 nm	28.5º	52,592 lbm[1]	n/a
-30 x 100 nm	51.6º	49,260 lbm[1]	n/a
100 x 100 nm	28.5º	n/a	105,487 lbm[2]
-2.6 km^2/sec^2	n/a	n/a	134,483 lbm
-2 km^2/sec^2	n/a	5146 lbm	133,585 lbm
0 km^2/sec^2	n/a	n/a	129,600 lbm
10 km^2/sec^2	n/a	n/a	111,262 lbm

Table 2: Performance and specifications for the Ares I and Ares V

(1) Ares I payload includes 10% performance margin, Payload provides circularization ΔV
(2) Ares V payloads to LEO orbits are based on a partially burned Earth Departure Stage (EDS)

The Ares V performance to the various values of C3, are based on a direct ascent trajectory and the complete exhaustion of the EDS propellant. Ares V performance to LEO in the preceding table is based on burning 290,000 lbm of EDS propellant in a sub-orbital burn with 218,519 lbm of propellant remaining. Propellant can be traded for payload in this configuration on a 1:1 basis, subtracting the added payload from the propellant remaining for an Earth departure burn.

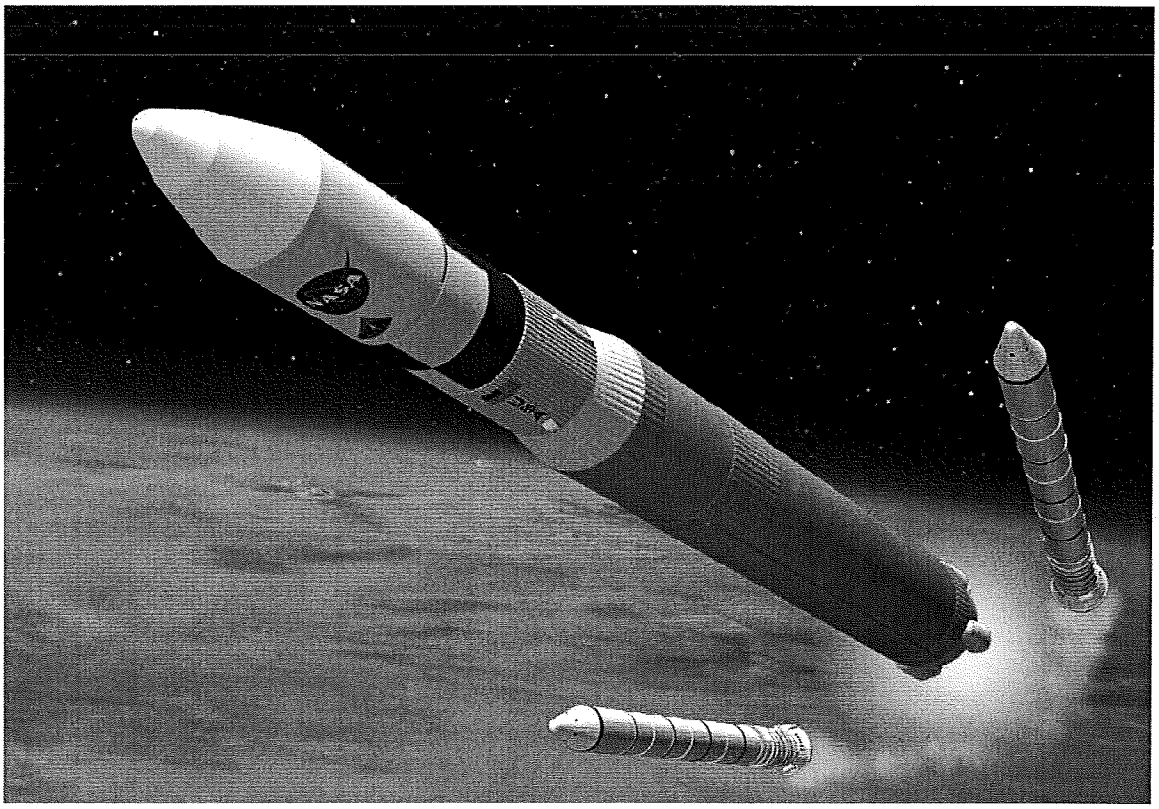

Figure 2: The Ares V Launch Vehicle at SRM Separation

V. Observer Description and Target Classification

The observer satellite is loosely based on the Deep Impact spacecraft. The observer uses several of the same payload instruments, with some additional instruments specifically designed to yield the maximum amount of information on the NEO. Whenever possible the payload package was selected to give multiple instruments capable of measuring each aspect of the NEO. A list of instruments on the observer satellite, and the measurements and results expected from each instrument can be found in Table 3.

The primary mission of the scout probe is to supply the critical information necessary for a successful diversion. The principal data goals are verification of mass and local dynamics (i.e. three dimensional rotations relative to the trajectory) as well as geometry and composition (i.e. solid, fragmented or rubble pile). This data needs to be gathered in time to provide the mission planners with targeting and timing parameters for the diversion. The philosophy behind the design is redundancy of approach to gathering the data and multi-purpose sensors. To provide the maximum mission flexibility, the main power source is assumed to be RTG. This will allow greater flexibility in maneuvering the spacecraft relative to the target without sun pointing or battery-life considerations.

Since the exact target and trajectory will not be known, a balance of capabilities and "delta v" must be made. How fast the target can be reached versus how long a sensing period will be available will be addressed in follow on studies. A baseline design uses the lift capacity of the ARES I together with proven technologies.

The primary sensors of the probe will be a 30cm optical system with an integral laser range finder and a MARSIS style subsurface radar sounder. In addition, the spacecraft will have on-board accelerometers/gravity sensors which when combined with range data from either radar or laser will provide mass estimates. The probe will also carry a lander and a box launcher for seismic impactors and gravity fly-by projectiles.

The optical system will have the laser transmitter(s) positioned in the shadow of the secondary and shared the 30 cm aperture (using a beam-splitter at the laser frequency) for the receiver portion of the range finder. The optical side will have both wide field and narrow field video systems with limited zoom

capabilities. The basic optical package, with associated electronics would be a common design with the diversion spacecraft targeting system as both missions have similar targeting accuracy requirements.

Category	*Instruments*	*Planned measurements*
Optical	Laser Ranger	Orbital elements
	Narrow Field CCD	surface mapping, geometry, dust environment
	Wide Field CCD	Dust environment, geometry, potential satellites
	Spectrometer	Composition, density
Radar	MARSIS radar sounder	Density, internal structure
	Dual mode radar/data link	Internal structure
Other	Gravity sensor	Mass, gravitational field

Instruments	*Planned measurements*
Chemical analysis package	Composition
Seismic sensor	Internal structure
Fly-by balls	Mass, Gravitational field

Table 3: Observer satellite instruments and expected measurements

The second mass determination method consists of launching a suitable mass (a shinny polished ball of aluminum) in a fly-by of the target. The laser ranger will supply velocity data and the optical system will track the sphere, the diversion of trajectory will be used to calculate the mass estimate. The box launcher, located on the central axis of the space craft will have a mix of seismic impactors and fly by spheres, thereby allowing multiple data acquisition attempts.

The lander will have a basic guidance system (similar to the diversion "bullets"), attitude control system and onboard command and control and data-link to the mother spacecraft.

The main sensor(s) of the lander are three seismic sensors on the three (fairly long deployable) legs with spikes to establish a close contact with the hard surface of the target. Due to the low gravity, it is anticipated that a constant thrust motor will be required to hold the lander against the surface while the mother craft launches a series of impactors into the target. The seismic sensors will monitor the internal reflections, giving us a view of the structure. A solid rock will have one pattern, a collection of large masses will have a different pattern and a pile of rubble will have no internal signal. Together with the radar mapping of much of the interior and modeling of the external geometry from the video system, a detailed picture of the target can be developed.

The basic spacecraft will require a fairly robust attitude control and star tracking (or sun –earth tracking system) to locate itself in space. It is anticipated that the main up-link/down-link would be a gimbaled hi-gain (parabolic) antenna, to allow the craft's sensors to be aligned with the target while transmitting data to earth. A second smaller hi-gain antenna would be on the sensor side of the craft, to communicate with the lander and as a dual purpose radar system/ranger as backup to the optical system. This second (smaller) hi gain could be the backup down link to earth, but would require reorienting the space craft to transmit/receive.

The optical system could also have a "DEEP IMPACT" style spectrometer to look at the ejecta from the impactors and the lander could have LOCAD style chemical analyzers built into the spikes.

Since the target may be tumbling relative to the mother-craft during the lander portion of the mission, the lander will require data storage and bust transmission capabilities and probably an omni-directional antenna.

Most of the technologies required for this mission already have been demonstrated and flown. The oil exploration industry has the seismic mapping technologies. The Mars probes have the radar mapping

technology. The image processing to calculate the rotation and geometry from the range and video stream (feature recognition and 2d-to-3d mapping from multiple images) already exists in various formats.

Observer Design

Attached below the observer satellite will be two different main propulsion system stages, one with a reaction control system; each stage either has its own subsystems or shares resources with the other stages. The stages produce enough ΔV to escape Low Earth Orbit (LEO) as well as perform any needed interplanetary maneuvers. The stages were sized so that they, in combination with the observer satellite, use the full capability of the Ares I as listed in Table 1. More detail about each of the stages is described in the upcoming sections of this report.

The configuration of the observer satellite and stages is shown in Figure 3. There were several constraints in laying out the vehicle configuration. Several payloads required unobstructed fields of view. Also there are typical constraints for avionics, thermal and propulsion systems. The propulsion stages were configured to minimize height to allow for the stack to fit within the Ares I launch shroud while maintaining simplicity. A more detailed explanation of the subsystems will be explained in following sections.

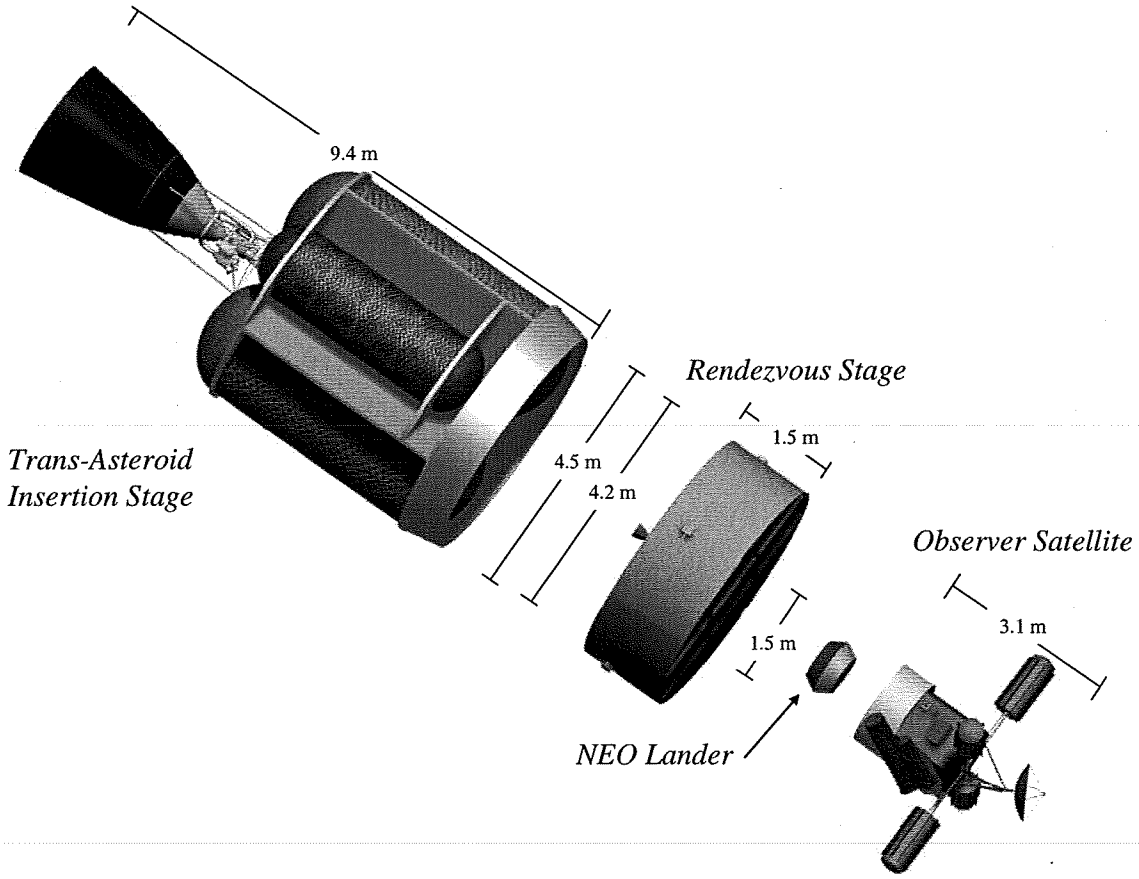

Figure 3: Observer satellite and kick stages.

Thermal subsystem

The observer satellite was represented in the thermal model with an outer thermal coating of AZW-LA-II low solar absorptance white paint ($\alpha/\varepsilon = 0.11/0.91$).

The thermal control concept for the Rendezvous Stage includes Aluminized Kapton or equivalent ($\alpha/\varepsilon = 0.46/0.81$) applied to the vehicle outer surfaces and Aluminized Mylar or equivalent ($\alpha/\varepsilon = 0.12/0.03$) applied to the vehicle inner surfaces. Each hypergolic propellant tank is overlaid with 50 layers of constant-density MLI. Propellant tank temperatures are maintained with a total of 15 Watts of heater power applied during LEO loiter and a total of 30 Watts during transit to rendezvous. The vehicle interior

is fully enclosed and neither the inner surfaces nor the propellant tank MLI outer layers receive any direct solar input.

The thermal control concept for the TAI Stage includes AZW-LA-II low solar absorptance white paint (α/ε = 0.11/0.91) applied to the vehicle outer surfaces and Aluminized Mylar or equivalent (α/ε = 0.12/0.03) applied to the vehicle inner surfaces. Each cryogenic propellant tank has a minimum-mass insulation design consisting of 0.5 inch of spray-on foam insulation (SOFI) applied to the tank's exterior wall and overlaid with 9 layers of variable-density multi-layer insulation (MLI). Propellant tank temperatures are maintained by thermodynamic venting of a total of 11.3 kg of propellant during an expected 6-hour LEO loiter. The vehicle interior is fully enclosed and neither the inner surfaces nor the propellant tank MLI outer layers receive any direct solar input.

Avionics subsystem

In the observer satellite, three computer modules are used for 2-fault tolerance. The computers are general purpose with 8 slots and PCI bus architecture. Each one contains all the circuit boards required to perform GN&C, data acquisition, image processing, actuator control, memory storage, and communication system interfacing. The processors used are a space qualified 132 MHz RAD750, which was flown on the Deep Impact asteroid observer and the Mars Orbiter Observer missions in 2005. They are latch-up immune, with a radiation hardness of 200Krads dose tolerance.

The navigation system uses 3 star trackers for flight and attitude control. They are Ball Aerospace advanced units CT-633, providing a lost-in-space recovery capability with 10 arcsec accuracy and a 6000 star catalog.

The communication system consists of a Ka-band High Gain Antenna (HGA) system with a 1 meter parabolic dish, and a 2-axis pointing platform. This system is used for ground communications, including uplink commands and data downlink. The in-space communication system consists of a 2-fault tolerant S-band system, which includes transceivers, transponders, and 3 omni-directional antennas for communications with the asteroid probe and Lander units. There is also a low gain system that is used as a back up system.

The Rendezvous and TAI stages are controlled and powered by the Observer portion of the stack. These stages contain instrumentation and cabling masses only under the avionics category in the WBS.

Structural subsystem

The structural model of the Rendezvous and TAI stages was analyzed together in the launch vehicle stack configuration. Maximum accelerations of 4.0g axial and 2.0g lateral were applied in order to insure the stages could withstand launch loads. Staging loads of -1.2g were also used. All Factors of Safety are in accordance with NASA-STD-5001.

Aluminum 2219 was used for all structural components, including tanks. All tanks were sized to withstand 50psi along with the affects of loads on the propellant. Tanks were analyzed as part of the structural model, but the results are book kept with the propulsion system.

Main Propellant Subsystem/Reaction Control Subsystem

In order to accomplish the initial Earth Departure burn, there is a LOX/LH2 stage. It was assumed that the CLV places the vehicle into a 100x100 nmi orbit and then the LOX/LH2 stage provides 4150 m/s, which is enough ΔV to escape Low Earth Orbit (LEO). It has one RL10 B-2 engine at a nominal Isp of 465.5 seconds, which is then de-rated by 1%. This stage is immediately jettisoned after the burn is completed.

The ΔV for the asteroid rendezvous maneuver is produced by a bi-propellant storable system which uses Hydrazine and N2O4 and a 1000 lbf thruster. This stage can provide up to 2000 m/s with an Isp of 330 seconds, which is de-rated 1%.

Last, there is a mono-propellant reaction control system which handles the additional ΔV requirements for interplanetary maneuvers, such as settling burns, mid-course corrections, attitude and directional control, and station-keeping. It pulls its propellant from the main propulsion system's hydrazine tank and has an Isp of 234 seconds, again de-rated 1%. This stage was sized to provide about 60 m/s.

Performance

Behind the observer satellite are two of liquid bipropellant stages. The stages produce enough ΔV to escape Low Earth Orbit (LEO) and for some additional ΔV for interplanetary maneuvers. The stages were

sized so that they, in combination with the observer satellite, use the full capability of the Ares I as listed in table 1. The performance of the stages is shown in Table 4.

Table 4: Performance of the TAI and Rendezvous kick stages for the observer satellite

Propulsion System	Thrust (lbf) / Number of Engines	Nominal Isp (seconds)	ΔV capability (m/s)	Propellant (kg)
LOX/LH2	24750/1	465.5	4150	13860
Hydrazine/N2O4	1000/1	330	2000	2165
Hydrazine	5/16	234	60	107

In order to obtain a one-way outbound trajectory for the observer satellite, the high thrust tool called MAnE, or Mission Analysis Environment which was developed by Jerry Horsewood of Space Flight Solutions, was used. After inputting such parameters as departure and arrival bodies (which were Earth and Apophis, respectively), specific impulse, approximate dates, and time of flight, the code gives ΔV values, burn times, V-infinity values, and optimizes the departure and arrival dates.

Three different opportunities were run; the spacecraft left in the years 2019, 2020, or 2021. Two different ΔV's were computed, that to leave Earth and that to rendezvous with Apophis. As was shown above, the upper bound of the rendezvous ΔV was ground ruled at 2000 m/s. This assumption eliminated the 2019 case. The 2020 and 2021 cases both still were plausible missions, even when considering the Trans-Asteroid Injection burn, which had an upper bound of 4150 m/s. However, note that the intention of this study was to keep the trajectory analysis as general as possible so the observer could leave at any point in time after the Ares I was built. In saying that, there are other windows after 2021 during which this spacecraft could launch, there was just not enough time in this study's schedule to run those other mission opportunities.

Mass Properties

The mass summary for the observer satellite is shown below. The structures and thermal masses were determined using percentages of the overall 1500 kg mass.

Table 5: Work Breakdown Structure (WBS) and mass properties for the observer satellite.

WBS Element - S/C & PL for Rendezvous			Qty	Unit Mass (kg)	Total Mass (kg)
	Structures				**400**
		Structures	1	300	300
		Mechanisms	1	100	100
	Thermal				**160**
		Thermal	1	160	160
	Power				**272**
		PMAD	1	32	32
		RTG	4	60	240
	Astrionics				**322**
		Avionics	1	73	73
		Communications	1	76	76
		Science Instruments	1	173	173
	Growth			-	**346**
		Structures	30%	-	120
		Thermal	30%	-	48
		Power	30%	-	82
		Avionics	30%	-	97
Dry Mass					**1500**
	Non-Cargo				**0**
	Cargo/Payload				**0**
Inert Mass					**0**
	Non-Prop Fluids				**0**
Total Less Propellant					**1500**
	Propellant				**0**
Gross Mass					**1500**

The mass summary for the rendezvous stage is listed in Table 6. It contains a list of the subsystem components as well as the quantity and unit mass for each. Lastly, the mass growth was assumed to be 30% for this stage.

Next is the mass summary for the Trans-Asteroid Injection (TAI) stage is listed in Table 7. It again contains a list of the subsystem components as well as the quantity and unit mass for each. The mass growth was 30%, like the rendezvous stage.

Table 6: WBS and mass properties for the rendezvous stage

WBS Element - Rendezvous Stage	Qty	Unit Mass (kg)	Total Mass (kg)
Structure			**352**
Primary Structures	1	352	352
Propulsion			**244**
Main Engines	1	22	22
Main Fuel Tank	2	11	22
Main Oxidizer Tank	1	12	12
Pressurization System	1	150	150
Feed System	1	29	29
RCS Engines	16	1	10
Environment			**12**
Thermal Control	1	12	12
Growth		-	**182**
Structure	30%	-	105
Propulsion	30%	-	73
Evironment	30%	-	4
Dry Mass			**790**
Non-Cargo			**77**
Residuals			*68*
Fuel	1	38	38
Oxidizer	1	30	30
Pressurant			*9*
Fuel	1	6	6
Oxidizer	1	3	3
Cargo/Payload			**1500**
Spacecraft	1	1500	1500
Inert Mass			**1577**
Non-Prop Fluids			**0**
Total Less Propellant			**2368**
Propellant			**2272**
Main and RCS Fuel	1	1278	1278
Main Oxidizer	1	995	995
Gross Mass			**4640**

VI. Interceptor Configuration

The interceptor proposed here is comprised of several elements. The individual technology options are integrated into a "bullet", sized so that six of them will fit into a single cradle. The cradle is standardized, so that one cradle will accommodate the entire interceptor technologies proposed herein. The cradle and bullets are propelled towards the NEO with a liquid bipropellant stage. As with the observer, the stage is sized so it and the cradle with the bullets will fully utilize the capabilities of the Ares V.

Figure 5Figure 4 illustrates the cradle, stage and a set of generic bullets. Shown in Figure 4 is views of the cradle in the stowed configuration and after release of all bullets. The performance and specifications of the cradle and stage are shown in table 4.

Table 7: WBS and mass properties for the TAI stage.

WBS Element - Trans-Asteroid Injection Stage	Qty	Unit Mass (kg)	Total Mass (kg)
Structure			**1559**
Primary Structures	1	1559	1559
Propulsion			**1316**
Main Engines	1	152	152
Main Fuel Tank	2	189	378
Main Oxidizer Tank	2	109	218
Fuel Tank CFM			*175*
MLI	1	5	5
SOFI	1	36	36
Thermodynamic Venting System	1	134	134
Oxidizer Tank CFM			*127*
MLI	1	3	3
SOFI	1	18	18
Thermodynamic Venting System	1	106	106
Main Pressurization System			*103*
MPS Fuel Pressurant System	1	69	69
MPS Oxidizer Press.System	1	34	34
Main Feed System			*163*
MPS Fuel Feed System	1	83	83
MPS Oxidizer Feed System	1	80	80
Power			**26**
Wiring Harness System	1	26	26
Avionics			**15**
Instrumentation	1	15	15
Other			**391**
Launch Vehicle Adapter	1	391	391
Growth			**992**
Structure	30%	-	468
Propulsion	30%	-	395
Power	30%	-	8
Avionics	30%	-	5
Other	30%	-	117
Dry Mass			**4298**
Non-Cargo			**518**
MPS Fuel Bias	1	19	19
MPS Bleed	1	45	45
MPS Residuals			*418*
Fuel	1	67	67
Oxidizer	1	352	352
MPS Propellant Boiloff			*11*
Fuel Boiloff	1	6	6
Oxidizer Boiloff	1	6	6
MPS Pressurant			*25*
Fuel	1	7	7
Oxidizer	1	18	18
Cargo/Payload			**4640**
Spacecraft	1	1500	1500
Rendezvous Stage	1	3140	3140
Inert Mass			**5158**
Non-Prop Fluids			**0**
Total Less Propellant			**9457**
Propellant			**13860**
Main Fuel	1	2132	2132
Main Oxidizer	1	11728	11728
Gross Mass			**23316**

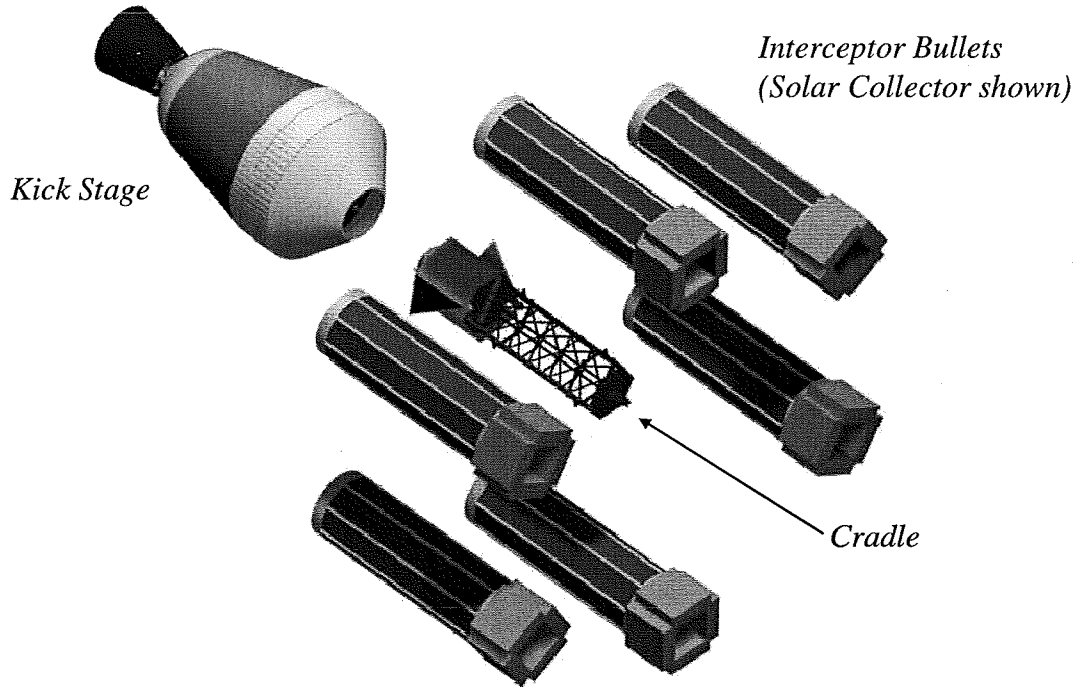

Figure 4: Exploded view of cradle, kick stage and solar collector bullets in unfolded condition.

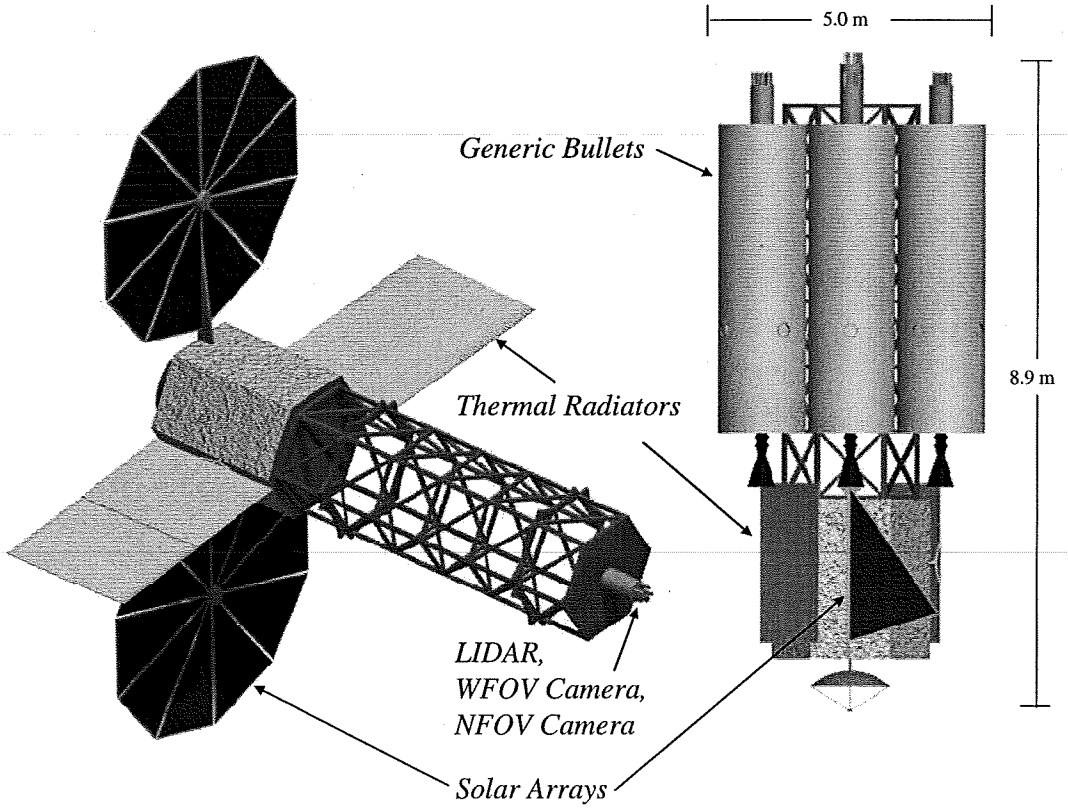

Figure 5: Cradle configurations. Stowed configuration with generic interceptor bullets (right); deployed configuration with no bullets (left)

Table 8: WBS and mass properties for the cradle kickstage

WBS Element - Cradle Kickstage			Qty	Unit Mass (kg)	Total Mass (kg)
	Cradle Kickstage				**3961**
		Burnout Mass	1	3961	3961
	Growth				**1188**
		Cradle Kickstage	30%	-	1188
Dry Mass					**5149**
	Non-Cargo				**0**
	Cargo/Payload				**11035**
		Cradle	1	11035	11035
Inert Mass					**11035**
	Non-Prop Fluids				**0**
Total Less Propellant					**16184**
	Cradle Kickstage Propellant				**29175**
Gross Mass					**45359**

Table 9: WBS and mass properties for the cradle

WBS Element - Cradle			Qty	Unit Mass (kg)	Total Mass (kg)
	Structures				**951**
		Structures	1	951	951
	RCS				**24**
		RCS Dry Mass	1	24	24
	Power				**272**
		Power	1	272	272
	Avionics				**239**
		Avionics	1	73	73
		Communications	1	76	76
		Instrumentation	1	90	90
	Thermal Control				**56**
		Thermal	1	56	56
	Growth				**463**
		Structures	30%	-	285
		RCS Dry Mass	30%	-	7
		Power	30%	-	82
		Avionics	30%	-	72
		Thermal	30%	-	17
Dry Mass					**2005**
	Non-Cargo				**0**
	Cargo/Payload				**9000**
		Interceptor	6	1500	9000
Inert Mass					**9000**
	Non-Prop Fluids				**0**
Total Less Propellant					**11005**
	RCS Propellant				**30**
Gross Mass					**11035**

The mass breakdown for both the cradle and cradle kickstage are shown above. The term "cradle kickstage" refers to the stage that gets the vehicle out of LEO, which provides 4650 m/s in addition to the 3940 m/s that the launch vehicle's Earth departure generates. This cradle kick stage consists of a LOX/LH2 propulsion system and carries all six of the interceptors and their cradle. After it completes its burn, it is jettisoned and any remaining burns are either performed by the RCS on the cradle itself or by the one of the engines on the bullets. The cradle kickstage was sized using a propellant mass fraction of 0.85.

The next component to be sized was the cradle. It was assumed the cradle holds six bullets as well as some other hardware, such as a LIDAR and cameras for observation and a reaction control system for attitude control. The avionics and communication package is similar to the Observer, since it has similar GN&C requirements. Above is a more detailed summary of the cradle mass that was named on "Cargo/Payload" line in the cradle kickstage.

VII. Interceptor Technology Options

The study assumes three possible technologies for mitigation of the NEO threat. These technologies include nuclear deflection, kinetic interceptor, and solar collector. Each of these options, their performance, and the designs for each technology is listed below. These technologies were selected as they are a representative subset of the wide array of options proposed in the literature for NEO mitigation. The nuclear option allows for high energy interaction with the NEO. The solar electric propelled kinetic interceptor delivers less energy, but with much more flexibility in achieving the optimum deflection angle. Finally the solar collector option delivers a very low power interaction with the NEO, but has the ability to sustain that interaction for months or years at a time.

Nuclear Interceptor

The inclusion of the nuclear option should not be interpreted as advocation or to opposition to further nuclear proliferation in space. Other venues are better suited for this debate. Furthermore, we recognize the facts that nuclear proliferation is occurring and probably will continue into the foreseeable future; and that in the event of a surprise detection of an inbound threat, political expediency may lead to one or more nations attempting to employ non-optimized nuclear countermeasures. Hence, we shall limit this discussion to examining the technical feasibility of using a nuclear device to deflect a hazardous object. Furthermore, we offer the strong recommendation that the deployment of any nuclear option be preceded by a dedicated mission planning and hardware development program to fully optimize the system for the mission.

In the event of a last minute scenario, the Hollywood solution of shooting several ICBM's at the incoming rock is fraught with danger. Recognizing that the launch capabilities are relatively limited, if an intercept were successfully achieved and if a successful release could be accomplished close to or on the asteroid, the interaction would occur relatively near the Earth. And, due to the associated masses and kinetic energies, it probably would not be sufficient to prevent impact raising the additional hazard of radioactive materials from the blast being introduced into the atmosphere. Fragmentation might be achievable. However depending on the composition of the incoming rock this may make things worse. For example, would we wish to fragment an object that was going to impact in a desert when the fragments might then fall on a city?

The approach used would be a stand-off nuclear release at the optimum height and coordinates above the object. A stand-off release offers several advantages. First, it is less likely to cause unpredictable fragmentation especially significant if the target is a rubble pile. And, it works no matter what the rotational characteristics of the object may be. Also, since in principle the energy may be released at any point relative to the target, the optimum delta v may be achieved on a flyby trajectory. Since orbit matching and docking are not required, substantively more payload may be dedicated to deflection capability.

A nuclear release above the surface of the object bombards it with hard x-rays, gamma rays, and neutrons. This pulse of energy is so fast that the material in the object's surface simply does not have time to radiate or conduct away the heat. Instead, a hot, rapidly expanding plasma is created that rapidly expands and escapes into space. We are essentially creating a crude rocket in that momentum is now transferred to the remaining mass of the object. The momentum transfer yields a ΔV.

Nuclear Interceptor Effectiveness

An optimum release involves the non-trivial operation of a maximum energy release accomplished at the optimum coordinates and time. Figure 6 illustrates the expected ΔV imposed on an asteroid of varying diameter for a 1 MT explosion. As will be seen in the nuclear interceptor design, the included B83 warhead is capable of a variable yield up to 1.2 MT. Thus the figure below represents a conservative estimate of the effectiveness of the nuclear interceptor design in this study. As mentioned above the cradle is capable of carrying up to six bullets each with its own warhead. Hence, multiple warheads not only increase system reliability, but also serve to increase the cumulative delta v and decrease the time needed before expected impact to achieve success.

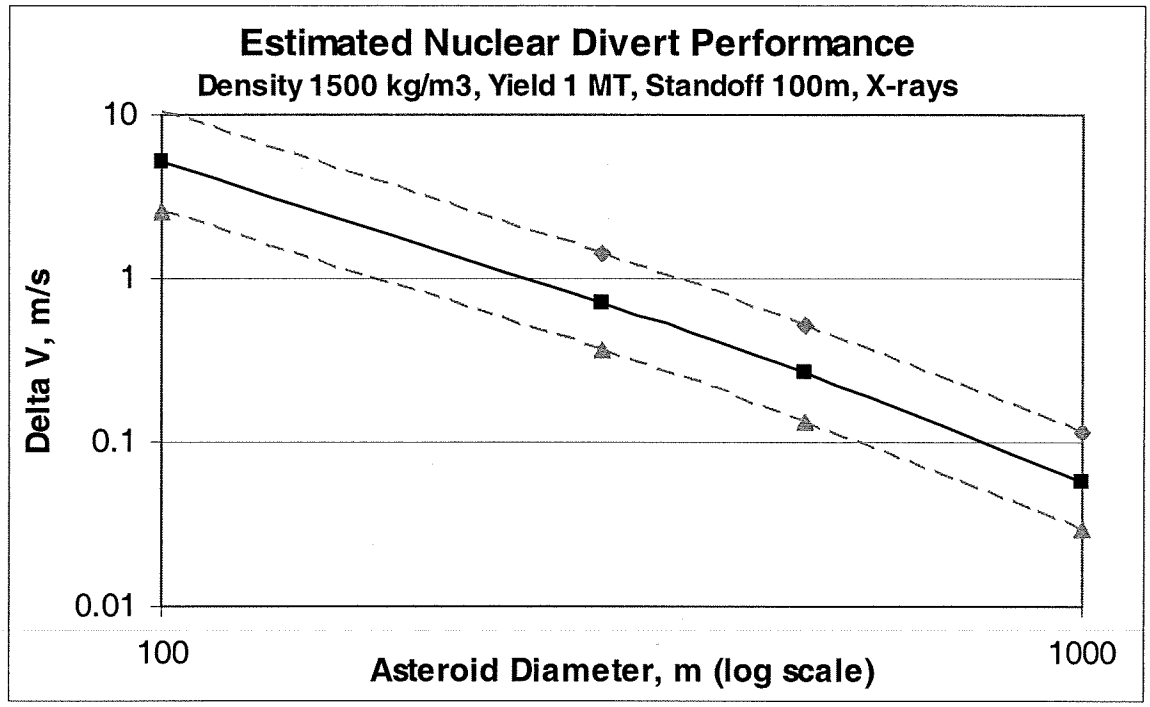

Figure 6: Performance of nuclear interceptor bullet as a function of asteroid diameter.

The analysis underlying the above figure has several sources of uncertainty. All the data contained in this study comes from publicly available sources, thus there is considerable uncertainty in the energy release and spectrum for a nuclear warhead. The analysis depends on only X-ray interaction with the asteroid. Neutron interaction is neglected as it is more difficult to predict spectrum and interaction with the asteroid, and that neutron interaction will occur after X-ray interaction. Actual X-ray absorption coefficients and mechanisms are conjectural given the uncertainty of asteroid compositions. For similar reasons the absorption vs. reflection distribution is dependant on asteroid composition. Finally the asteroid density and shape, as well as its roughness will affect the direction of blow-off and the net force acting on the asteroid

Terminal Rendezvous Package

The terminal rendezvous package consists of the instrumentation necessary to guide the nuclear interceptor to its detonation point near the NEO (about one-third the diameter of the NEO). The key components of the terminal guidance package are a Wide Field of View (WFOV) Visible/Near Infrared (Vis/NIR) Imager, a Narrow Field of View (NFOV) Visible/Near infrared (Vis/NIR) Imager and a Light Detection and Ranging (LIDAR) Device. The terminal rendezvous package is designed around instruments, which have flown on other NASA missions, or is similar to such instruments. This is the approach taken by Barrera[3] in his paper, "Conceptual Design of An Asteroid Interceptor for a Nuclear Deflection Mission," and is a reasonable set of sensors to baseline for this interceptor design. Specifications for the imagers are found in Table 10 below.

Table 10: Specification for WFOV and NFOW imagers.

Parameter	WFOV Imager	NFOV Imager
Acquisition Range (km)	~5000	~5000
Field of View (deg)	9.5x9.5	2.3x2.3
Angular Res. (μrad)	40	10
Focal Plane (pixels)	1024x1024	1024x1024
Effective Aperture (cm)	2.1	8.5
Effective Focal length (cm)	22.3	90
Estimated Mass (kg)	10	15
Heritage Instruments	NEAR Vis/Nir Imager	DS-1 MICAS

The LIDAR needs to have sufficient power to operate over a range equivalent to approximately the last minute of the homing phase. For closing velocities of 5 km/s to 10km/s, this would require a range of around 5000 km. This could be something on the order of the instrument designed for the NEAR and Clementine[4] missions.

The interceptor uses the WFOV Imager for acquisition of the NEO at the beginning of the homing phase, which begins about 5000 km from the NEO. The handover coordinates for the NEO are given to the interceptor by the more powerful visible and radar sensors on the bus via its communications link. The field of view of the WFOV Imager is approximately 10 deg x 10 deg to allow for uncertainties in the hand-over coordinates from the bus.

As soon as possible after acquisition of the NEO, the WFOV Imager hands over to the NFOV Imager, which has a field of view of 2.3 deg x 2.3 deg. This Imager, with its higher resolution, provides successive images of the NEO to the flight computer where navigation algorithms are used to calculate the course corrections necessary to guide the interceptor to its intercept point. The computer then uses these calculations to provide inputs to the divert and attitude control systems which provide the thrust to keep the interceptor on course to the intercept point.

The baseline navigation algorithms will be similar to the AutoNav[5] algorithms used to guide the Impactor spacecraft to a successful impact on the comet Tempel-1 during the Deep Impact mission. If data gathered during the Observer flight to the NEO should indicate that a more robust set of navigation algorithms would be desirable, given the characteristics of the NEO, algorithms used in current tactical interceptor programs could be adapted for this purpose.

The LIDAR will be used in the closing seconds of the homing phase to determine the range to the NEO so that detonation of the nuclear devise can occur at the proper distance from the NEO for maximum effect on the NEO. Since the stand-off distance for detonation is about one-third the diameter of the NEO, range resolution of the LIDAR should be on the order of one or two meters.

The interceptors are designed to have a mass of 1500 kg including fuel. Each interceptor will have 0.75 km delta V including the delta V required to provide one hour of separation between the six interceptors after they are separated from the bus. The one-hour separation between detonations is necessary to provide clearing of debris and to ensure that the nuclear detonations do not interfere with each other. Each interceptor will have a minimum of 200 m of delta available for use during the homing phase of the interceptor's flight.

Figure 7 shows the amount of delta V required to correct for 1 km of trajectory error, or miss-distance for different ranges to the NEO. As can be seen from the chart, the delta V required to correct for a given error is less the further out the correction maneuvers begin. An error of up to 100 km can be removed with the available 200 m/s of delta V for closing speeds up to 10 km/s if corrections can begin at 5000 km. For errors less than 100 km or closing speeds less than 10 km/s, the delta V requirements become less stressing.

Nuclear Interceptor Design

The individual bullets for the Nuclear Interceptor were analyzed. There are six of these interceptors, each weighing 1500 kg, for a total of 9000 kg. This mass is book-kept with the "Cargo/Payload" line in the table above. The table below calls out each piece of hardware that was sized for a more in-depth look at what is included on each interceptor. Note that the TRP stage and the interceptor kickstage were sized with propellant mass fractions of 0.80 and 0.85, respectively.

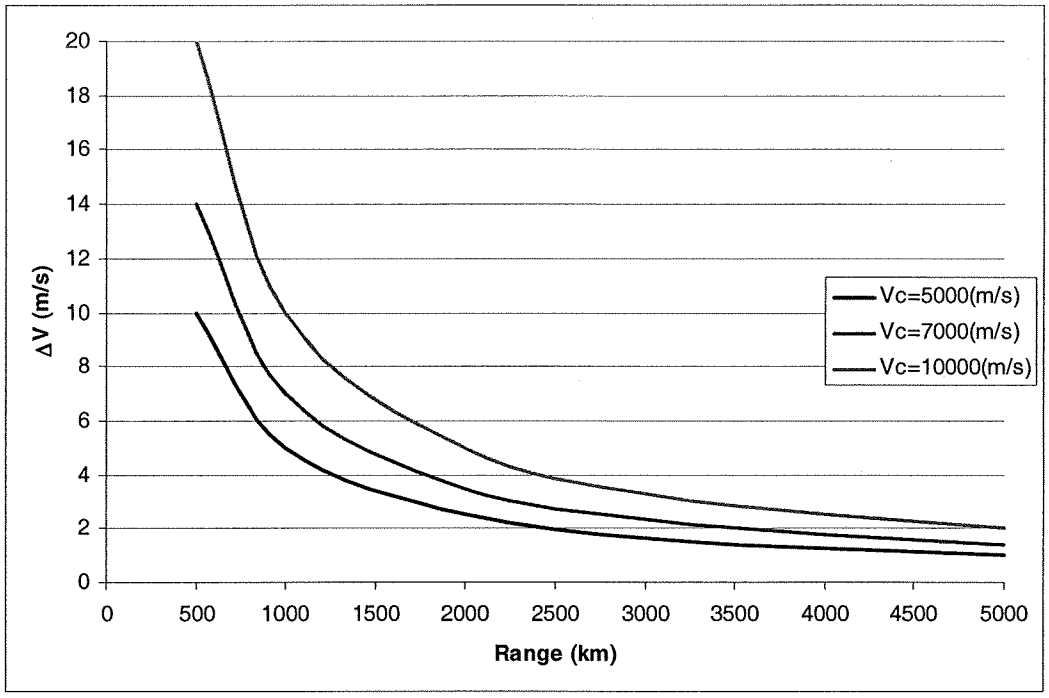

Figure 7: ΔV requirements for terminal intercept as a function of closing speed and range at acquisition. Terminal intercept package is sized assuming worst case scenario of 10 km/sec closure and acquisition at 5000 km.

Table 11: WBS and mass properties for the nuclear interceptor bullets

WBS Element - Nuclear Interceptor			Qty	Unit Mass (kg)	Total Mass (kg)
	TRP Sensors				**90**
		WFOV Imager	2	10	20
		NFOV Imager	2	15	30
		LIDAR	2	20	40
	TRP Stage				**33**
		Burnout Mass	1	33	33
	Interceptor Kickstage				**56**
		Burnout Mass	1	56	56
	Growth				**54**
		TRP Sensors	30%	-	27
		TRP Stage	30%	-	10
		Int Kickstage	30%	-	17
Dry Mass					**233**
	Non-Cargo				**0**
	Cargo/Payload				**913**
		Nuclear Warhead	1	913	913
Inert Mass					**913**
	Non-Prop Fluids				**0**
Total Less Propellant					**1146**
	TRP Propellant				**104**
	Interceptor KS Propellant				**250**
Gross Mass					**1500**

As can be seen from Figure 8, the nuclear interceptor is comprised of the terminal intercept package, the nuclear warhead, and the main engine. The main engine is sized to provide 0.4 g's of thrust for a maximum ΔV of 0.55 km/s. This propellant load is sufficient to accelerate the first bullet to a speed sufficient to allow it to strike five hours before the final bullet. Thus all six bullets can accelerate to the appropriate speed so that the warheads explode in intervals of one hour. The fuel load and thrust capability allows for the bullets to space themselves out in 1 hour intervals if they have been released at least 100 hours before the cradle intercepts the asteroid. Finally both the main engine and the terminal intercept engines operate on hydrazine and N2O4. Both propulsion systems feed from the same set of tanks.

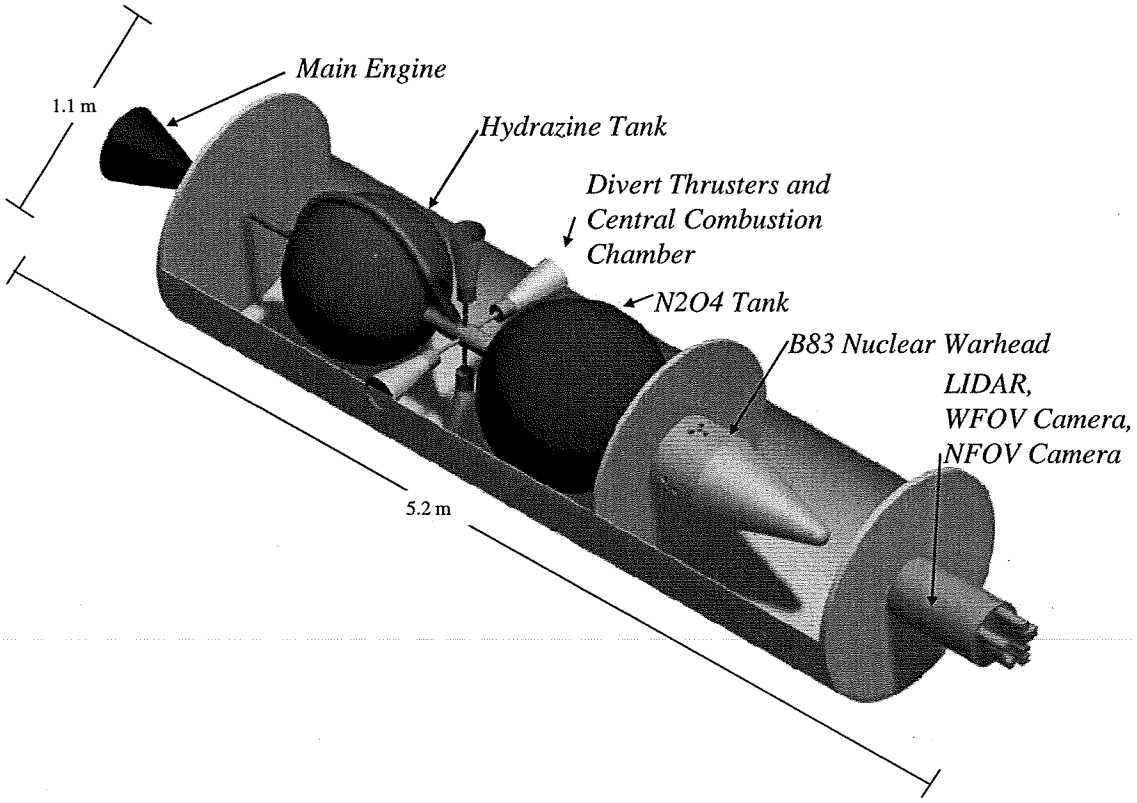

Figure 8: Illustration of the nuclear interceptor bullet with major dimensions and subsystems indicated.

Kinetic Interceptor

In this section we study how to avoid the asteroid's fragmentation during the kinetic impact by the bullet. This problem was first faced by Thomas J. Ahrens of Caltech and Alan W. Harris of JPL back in 1994 ([1]Ahrens, T. J, and Harris, A. W). Ten years later, their equations were embodied in the NASA/TP – 2004-213089[2] and also coded in the form of an Excel spreadsheet. Finally, in January-February 2007 co-author C. M. converted that Excel spreadsheet in MathCad form and used the equations given by Ahrens and Harris, as well as by Adams et al., to produce the results described in this section. In the sequel, the Kinetic Impact will be abbreviated KI and the bullet will rather be called "the bullet", because this is… what it is!

Kinetic Interceptor Effectiveness

Let us start by pointing out that, in the NASA/TP of 2004, the condition for non-fragmentation or fragmentation of the asteroid is that the ratio of the kinetic energy of the bullet to the asteroid's mass must be smaller or larger than 0.5 joules/gram, respectively. In other words, denoting the bullet's kinetic energy by E_{bullet}, the condition for non-fragmentation (called condition for craterization also) reads

$$\frac{\frac{E_{bullet}}{M_{asteroid}}}{\frac{joule}{gram}} < 0.5 . \quad (1)$$

The kinetic energy of the bullet is given by

$$E_{bullet} = \frac{1}{2} m_{bullet} v_{bullet}^2 . \quad (2)$$

Clearly, v_{bullet} is the kinetic energy of the bullet in the reference frame centered at the asteroid's center-of-mass, i.e. the reference frame in which the asteroid is still before the bullet's impact. Then, replacing Eq. (2) into Eq. (1) and replacing the numeric factor 0.5 by ½, the non-fragmentation condition (1) becomes

$$\frac{\frac{1}{2} m_{bullet} v_{bullet}^2}{M_{asteroid}} < \frac{1}{2} \cdot \frac{joule}{gram} . \quad (3)$$

Solving this for v_{bullet}, one gets the final expression of the no-fragmentation condition or craterization condition

$$v_{bullet} < \sqrt{\frac{M_{asteroid}}{m_{bullet}}} \cdot \sqrt{\frac{joule}{gram}} . \quad (4)$$

In other words, if we want to be sure that only craterization and no fragmentation of the asteroid will occur in the KI process, the bullet must reach the asteroid with speeds that are below, or far below the following maximum bullet speed

$$v_{Max\_bullet}(M_{asteroid}) = \sqrt{\frac{M_{asteroid}}{m_{bullet}}} \cdot \sqrt{\frac{joule}{gram}} . \quad (5)$$

If we plot this function as a function of the asteroid mass $M_{asteroid}$ we clearly get the craterization condition for the full range of sizes that asteroids have, from meters to kilometers. However, asteroids also vary in density, and not just in size. Thus, to also take the density into account, we must replace the asteroid mass in Eq. (5) (further assuming the asteroid shape to be spherical in order to simplify things) by

$$M_{asteroid} = \rho_{asteroid} \cdot \frac{4}{3} \pi \cdot \left(\frac{D_{asteroid}}{2} \right)^3 . \quad (6)$$

That yields the new maximum-bullet-speed function

$$v_{Max\_bullet}(D_{asteroid}, \rho_{asteroid}) = \sqrt{\frac{\pi}{6}} \cdot \sqrt{\frac{\rho_{asteroid}}{m_{bullet}}} \cdot \sqrt{\frac{joule}{gram}} \cdot D_{asteroid}^{\frac{3}{2}} . \quad (7)$$

The density of all asteroids almost always lies in between 1 gram/cm^3 and 4 gram/cm^3. Therefore we may regard $\rho_{asteroid}$ in Eq. (7) as a "parameter" and plot the same function (7) four times on the same plot for different asteroids densities. The result is Figure 9, where the four colors refer to densities of 1 gr/cm^3 (green), 2 gr/cm^3 (red) (somehow the most likely value), 3 gr/cm^3 (magenta) and 4 gram/cm^3 (blue). To fix the ideas, the mass if the bullet, m_{bullet}, is supposed here to be 1500 kg, but of course Eq. (7) could be re-plot for any m_{bullet} value.

In the practice, the actual impact speeds of a 1500 kg bullet against the asteroid will be of the order of 10 km/s, i.e. much smaller than the above values except for "very small" asteroid sizes, like 70 meters or so. Let us explore this topic more in detail. Figure 10 shows the same curves shown by figure 1 for the "small" asteroid sizes up to 70 meters. In addition, we plotted the horizontal black solid curve of impact speed of 10 km/s. The question is: at which values of the asteroid size do the four growing curves intercept the constant 10 km/s black curve?

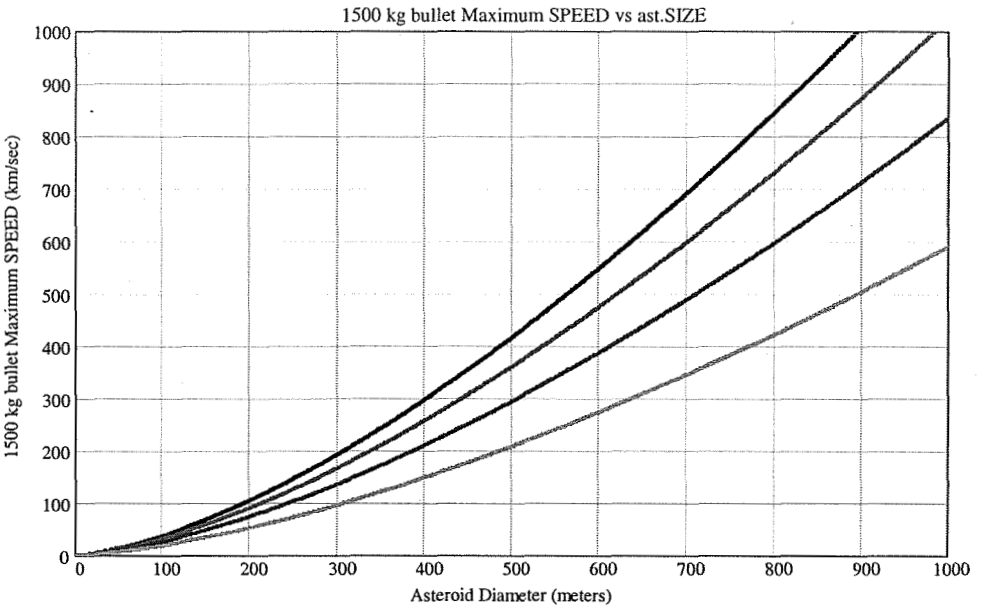

Figure 9: Maximum bullet speed to avoid fragmentation of the target asteroid vs. the asteroid size for asteroids ranging in between 0 and 1 km in diameter. The lower curve refers to asteroids having a density of 1 gr/cm^3, the second curve 2 gr/cm^3, the third curve 3 gr/cm^3 and the fourth one 4 gr/cm^3.

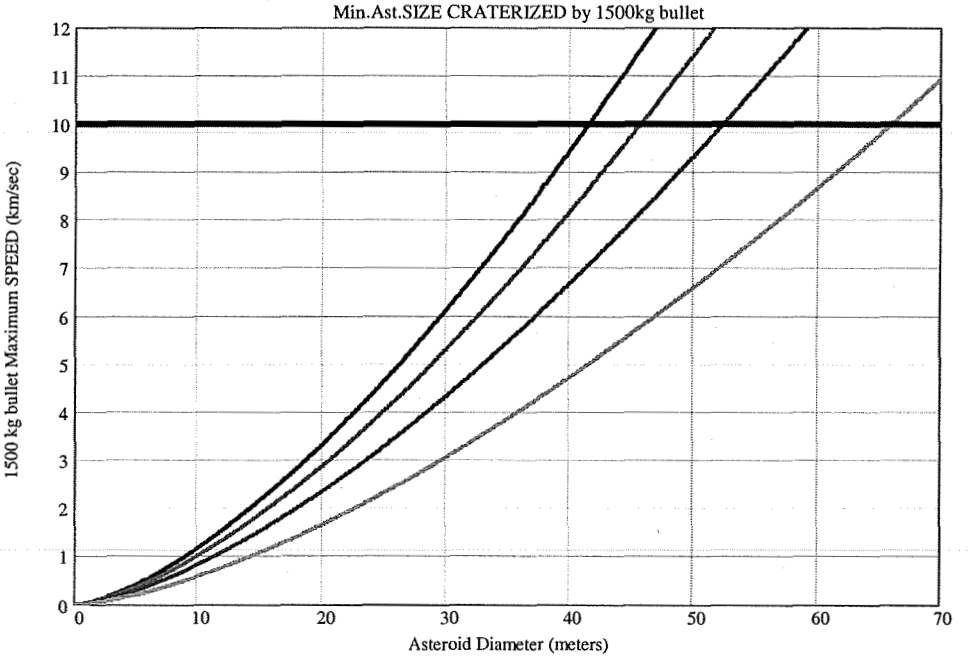

Figure 10: Minimum asteroid sizes for which craterization (and not fragmentation) is still achievable by virtue of a 1500 kg bullet impacting the asteroid at the speed of 10 km/s (black solid line). The numerical values of the four intercept points between the growing curves and the horizontal solid line at 10 km/s are, respectively, from left to right: 41.528 meters, 45.708 meters, 52.322 meters and 65.922 meters. The "safe" craterization region lies BELOW the growing curves and the black horizontal line. Above it, the asteroid would be fragmented by the bullet.

The answer is found firstly by solving Eq. (7) for D_{NEO}, that is

$$D_{NEO} = \sqrt[3]{\frac{6}{\pi}} \cdot \sqrt[3]{\frac{m_{bullet}}{\rho_{NEO}}} \cdot \sqrt[3]{\frac{gram}{joule}} \cdot \sqrt[3]{\left(v_{Max\_bullet}\right)^2} \,. \tag{8}$$

Secondly, we must replace v_{Max_bullet} in Eq. (8) by the value of 10 km/s. For the different four values of the asteroid density, we then get the four asteroid sizes (with densities in decreasing order, from 4 grams/cm3 to 1 gram/cm3): 41.528 meters, 45.708 meters, 52.322 meters and 65.922 meters. Please notice that Humanity must deflect even asteroids as "small" as these ones because they would create craters like the "Meteor Crater" in Arizona. This deflection can be achieved by shooting against them bullets with mass of 1500 kg, but the problem is more complicated for the "smaller" asteroids (i.e. less than 70 meters in diameter) because the risk to fragment the asteroid becomes real. The only way to avoid this fragmentation risk is to shoot bullets at speeds lower than 10 km/s! A trade-off difficult indeed! And there are much more "smaller" asteroids than "larger" asteroids.

Finally, let us pursue the calculation of the ΔV that the asteroid undergoes when hit by the bullet. Assuming (for the sake of simplicity, but a more profound investigation is certainly needed) inelastic conservation of momentum, from the simple equation

$$\Delta v_{asteroid} \cdot M_{asteroid} = v_{Max\_bullet} \cdot m_{bullet} \tag{9}$$

(by words: the asteroid is displaced from the origin of the reference frame it occupied before the bullet's impact!), solving for $\Delta v_{asteroid}$ one gets

$$\Delta v_{asteroid}\left(D_{asteroid},\ \rho_{asteroid}\right) = \sqrt{\frac{6}{\pi}} \cdot \sqrt{\frac{m_{bullet}}{\rho_{asteroid}}} \cdot \sqrt{\frac{joule}{gram}} \cdot \frac{1}{D_{asteroid}^{\frac{3}{2}}} \,. \tag{9}$$

The set of these four curves is plotted in Figure 11.

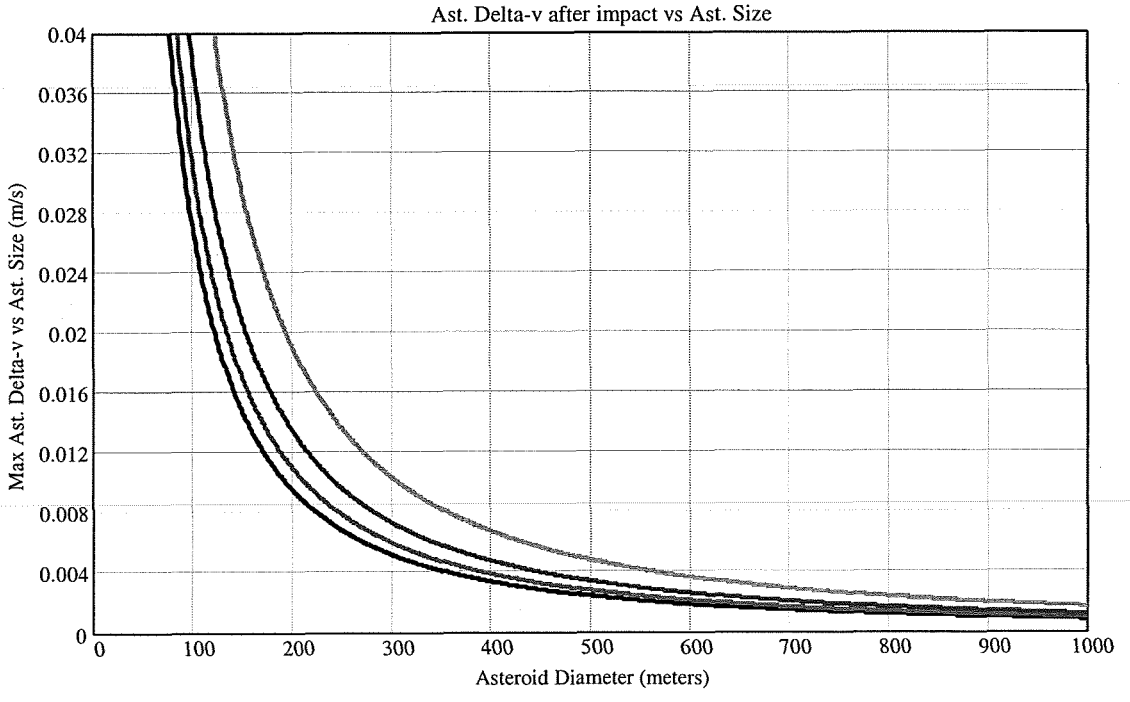

Figure 11: Asteroid ΔV after KI for asteroids up to 1 km in size. The ΔV are of the order of millimeter/second for asteroids larger that about 300 meters. But they increase to cm/s for asteroids smaller than 300 meters.

Again the "smaller" asteroids deserve special interest! Just re-plot the same curves as before for asteroids smaller than 100 meters, as plotted in Figure 4. We then see that the ΔV increases to decimeters/second around 50 meter in diameter (Meteor Crater like), and even to 1 meter/second for rocks of the size of 10 meters. It should be reminded here that only rocks smaller than 3 meters are supposed to be destroyed by the attrition with the atmosphere, whereas rocks larger than 3 meters would still hit the ground or the sea, causing considerable damage in land sizes as large as a town block.

Kinetic Impactor Design

The Cradle Kickstage and the cradle to hold the impactors were the same designs that were used in the nuclear interceptor option so those mass summaries apply to this case too. However, the individual bullets for the Kinetic Interceptor had to be specifically designed for this mitigation option. There are six of these interceptors, each weighing 1500 kg, for a total of 9000 kg. The table below calls out each piece of hardware that was sized for a more in-depth look at what is included on each interceptor.

Table 12: WBS and mass properties for solar electric propelled kinetic interceptor

WBS Element - Kinetic Impactor			Qty	Unit Mass (kg)	Total Mass (kg)
	TRP Sensors				**90**
		WFOV Imager	2	10	20
		NFOV Imager	2	15	30
		LIDAR	2	20	40
	TRP Stage				**33**
		Structure	1	17	17
		Thruster Pack	4	4	16
	SEP Stage				**653**
		Structure	1	190	190
		Xenon Tank	1	40	40
		Thrusters	2	64	128
		Solar Panels	2	105	210
		Avionics	1	16	16
		PMAD	1	70	70
	Growth				**233**
		TRP Sensors	30%	-	27
		TRP Stage	30%	-	10
		SEP Stage	30%	-	196
Dry Mass					**1009**
	Non-Cargo				**0**
	Cargo/Payload				**87**
		Kinetic Penetrator	1	87	87
Inert Mass					**87**
	Non-Prop Fluids				**0**
Total Less Propellant					**1096**
	TRP Propellant				**104**
	SEP Propellant				**300**
Gross Mass					**1500**

Note that the kinetic interceptor requires a terminal intercept package similar to that on the nuclear interceptor. The solar electric propulsion system allows the kinetic interceptor to maneuver to strike the asteroid from the optimum direction at the highest velocity possible (without exceeding the 10 km/s limit imposed by the terminal intercept system). The kinetic interceptor is illustrated in the figure below.

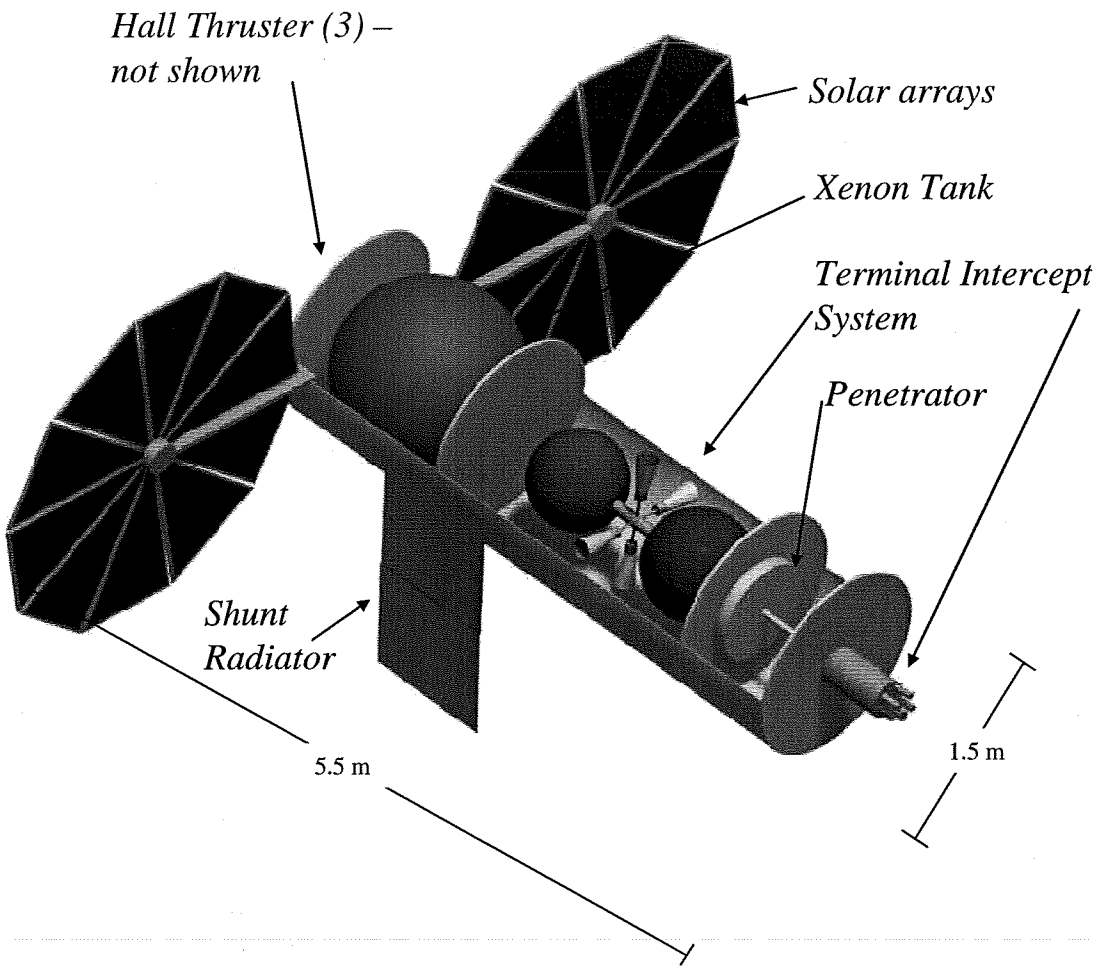

Figure 12: Illustration of the kinetic interceptor bullet with major dimensions and subsystems indicated.

Solar Collector

The solar collector, which maintains station near the NEO, consists of a 100-m diameter parabolic collector that faces the Sun and focuses sunlight onto a smaller thruster. The thruster directs the collected solar beam upon the NEO and has a fixed orientation relative to the Sun. As the NEO rotates beneath the solar collector, a swath of NEO material is continuously energized by the collected beam. Some of the energized NEO material evaporates into a jet, producing thrust and deflecting the NEO.

Solar Collector Effectiveness

The solar collector interaction with the asteroid is modeled after the algorithm developed in the last study[2].

The beam intensity incident on the object is assumed to be equal to that incident on the collector. This intensity is roughly 1375 W/m2 at one astronomical unit from the sun. All that is required is to determine the force imposed on the asteroid or comet by the incident beam.

The amount of mass ejected from the object is calculated as

$$\dot{m}_e = \frac{I(r)A_{sail}}{H_{vap} + \frac{v_e^2}{2}} \qquad (10)$$

where H_{vap} is the heat of vaporization (3 MJ/kg for water ice) and v_e is the velocity of the ejecta. As a first approximation the ejecta is assumed to come out at its sonic velocity (around 1 km/s). From this we can determine the force exerted on the object by the ejecta

$$F = \beta' \dot{m}_e v_e \quad (11)$$

Here β' is a gas expansion factor – assumed to be 0.5 – which represents a hemi-spherical expansion. Figure X below illustrates the expected acceleration that a single solar collector can impose on an asteroid using the above model.

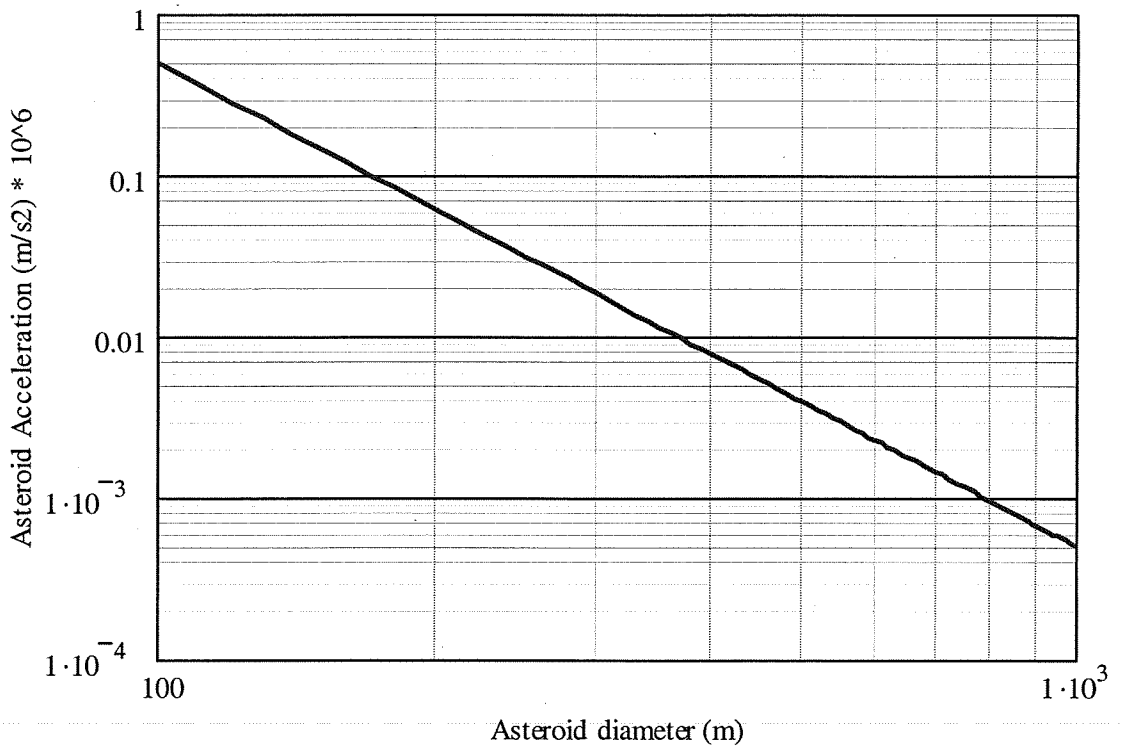

Figure 13: Asteroid acceleration as a function of asteroid diameter for the solar collector used in this study. Accelerations above assume an asteroid density of 1500 kg/m3.

Beam divergence is a major issue for this concept. Ejecta from the asteroid will adversely affect the operation of the collector, Additionally the solar collector will undergo a net acceleration from solar light pressure complicating stationkeeping near the asteroid. For these reasons the solar collector needs to affect the asteroid from a considerable distance away. As a rough calculation we can estimate the beam divergence as

$$\theta = 1.22\frac{\lambda}{D} \quad (12)$$

Where l is the wavelength of light and D is the beam diameter coming off the secondary. Solar radiation is approximated by a blackbody with a surface temperature of 5780 K, thus the solar spectrum covers the majority of the electromagnetic spectrum. However the peak wavelengths are in the visible spectrum, or around 500 nanometers. Given a secondary collector of 2m in diameter the wavelengths in the visible spectrum should experience a divergence of around 3E-7 radians. At a distance of 50 km these wavelengths would experience an increase in beam diameter of less than 1%. Of course larger wavelengths would experience higher beam divergences. More calculation is required, and already it is evident that expecting all of the solar energy collected on the primary to be concentrated at the hot spot on the asteroid is optimistic, but these calculations suggest that the loss to beam divergence is manageable.

Solar Collector Design

The design of the solar collector is substantially different than that for the other options. Once released from the cradle, the solar collector must inflate to its deployed size. Vanes running along seams in

the primary collector will fill with nitrogen, unfolding the primary collector. The primary collector membrane is made from materials similar to that for solar sails. Additionally guide wires from the primary hold the secondary collector in place. The secondary collector experiences a high luminous intensity, complicating thermal design, as discussed below.

Thermal subsystem

The primary collector is a thin-film membrane with very little thermal mass. The concave face of the primary collector must always point towards the sun, and thus the convex face always points towards deep space. Thus the primary collector thermally stabilizes to an acceptable temperature.

The secondary collector is assumed to be a beryllium panel electrochemically overplated with gold. This gives an average reflectivity of 98% of the solar flux over the solar spectrum. The absorbed flux is conducted through the collector material to the heat-pipe radiators, which are located on the back of the secondary collector. A 0.50m diameter sun-shield is placed 0.50m from the radiator. The sun-shield tracks the sun, providing continuous shielding for the radiator from a direct solar view. The radiator is assumed to radiate to deep space at an average temperature of 800K. This causes the working fluid to be potassium and the heat-pipe material to be niobium. The heat pipes will be oriented along the motion of the sun on the secondary collector as seen in Figure 14, allowing the beryllium panel to be thinner than if it was required to carry all the thermal expansion loads.

The tip vanes have minimal power dissipation requirements, so a small, double-sided radiator is used on each tip vane for thermal control.

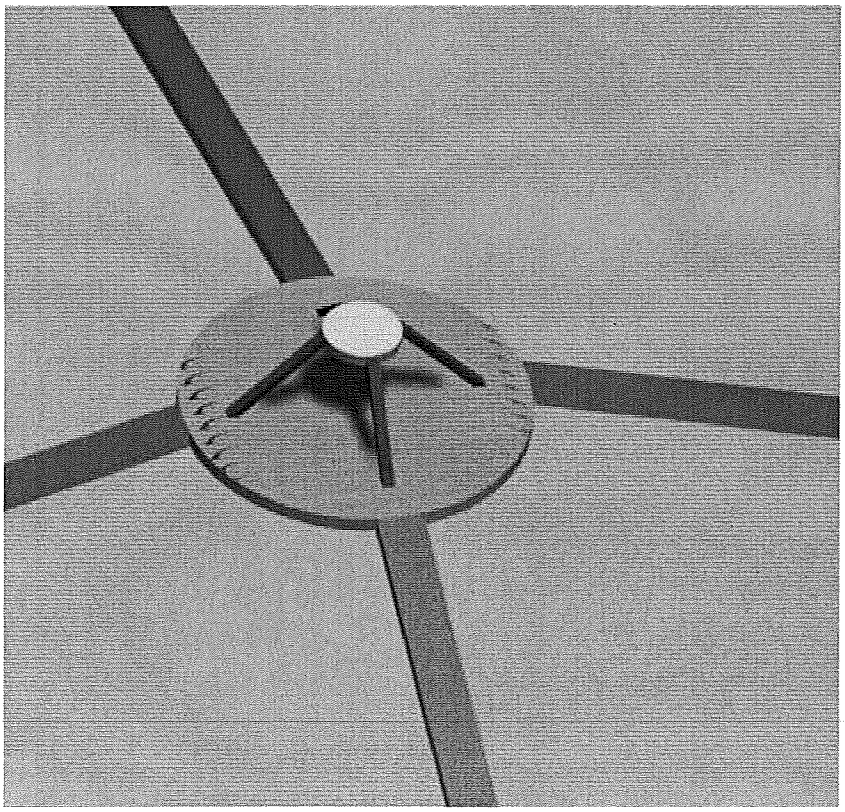

Figure 14: Detail view of secondary collector. Note sun shield and heat pipes.

Avionics subsystem

The avionics system consists primarily of the tip vane avionics and the secondary mirror avionics. The tip vane avionics is divided into a smart vane system and a remote controlled vane system, where two out of the four vanes are smart, and the other two vanes are remote controlled. The smart vanes will contain one general purpose RAD750 computer module each, that performs all GN&C functions along with actuator drivers and instrumentation and health monitoring circuits. Also, each smart vane will provide communications by a Ka-band high gain antenna system with a 0.5 meter pointing antenna, along with a

low gain S-band system for backup. Having two smart vanes at opposite ends of the collector should assure at least one of the vanes has an unobstructed line of sight to earth at all times for communication purposes. This same two vane configuration should also assure an unobstructed line of sight to the NEO for operations and imaging purposes. Therefore, the two smart vanes will also provide a platform for the imaging and ranging instrumentation. The instrumentation package consists of a NFOV and a WFOV camera for rendezvousing, tracking, and operational observation of the NEO, along with a LIDAR for accurate ranging information. In addition to the pointing capabilities, having the two tip vanes with independent avionics and instrumentation provides a single fault tolerance system.

Both the smart and remote controlled tip vanes are provided with a star-tracker for independent pointing capabilities. The remote vanes are connected to the smart vanes by a 1553 data bus, where the computers calculate the required pointing parameters of the remote vanes and send a pointing command to the remote pointing motors. The remote vanes also send health and status data to the computers using the 1553 data bus.

The secondary mirror avionics system was kept to a minimum since this is a hot environment. For this reason, there are no computers or thermally sensitive electronics placed in this area. Sun sensors are place on the sun shade. The sun shade has a dual use as the thermal electric generator. The sun sensors are used for continuously pointing the shade at the sun, and are connected by a 1553 data bus to the smart vane computers in the same way as the remote tip vanes.

Power subsystem

Power is provided by a thermopile consisting of 42 thermo-electric units, each unit consisting of 71 individual thermo-couples. The thermopile itself is encased in a conductive casing coated black on the 'hot' side and made reflective on the 'cool' side to produce a thermal gradient of 400K across the thermopile. This will yield an unregulated 24 A at 33.32 V to be regulated to a standard 28.8 V for a total of 691 W. Assuming a 5% regulation loss, the total delivered power is 656 W. Three hours of battery power was sized for power storage to operate the deployment and inflation mechanisms of the solar collector.

Structural subsystem

The structural subsystem for the solar collector consists of an inflatable primary structure used to support the primary and secondary collector. The structure is composed of thin film composite laminate beam truss which is deployed using an inflation system. Once inflated, the structure is cured in situ.

The mass properties for the solar collector are shown in Table 13. Also Figure 15 shows the major components of the solar collector system.

VIII. Analysis of NEO Deflection Requirements

The authors decided upon two computer applications for modeling the outbound and inbound trajectory legs for the deflection scenarios – Planetary Body Intercept (PBI) and Copernicus. PBI, which only considers impulsive maneuvers, was developed specifically for planetary body maneuvering analysis and was used in the previous study[2] to analyze the inbound planetary body trajectories. PBI reads from an input file the position and velocity vectors of the earth and planetary body at the time of impact, integrates the equations of motion backward in time by a user-specified number of days, and then determines the impulsive delta-v required to make the planetary body miss Earth by a specified distance. For this study, the specified distance was 3 Earth radii (or 4 Earth radii from Earth's center). The impulsive delta-v directions can be varied, but given the study schedule and results from the previous study,[2] the only directions analyzed for the impulsive deflection maneuvers were parallel to the planetary body's velocity vector, either in the same direction as the velocity vector or in the exact opposite direction. These maneuvers, specified with the keywords ACCEL or DECEL in the input file for PBI, generally result in the lowest delta-v requirement. The gravitating bodies included in the model are the sun and the earth. The effect of the moon is not considered.

Copernicus is a generalized spacecraft trajectory design and optimization program developed by the Trajectory Optimization Group in the Department of Aerospace Engineering and Engineering Mechanics at The University of Texas at Austin. Copernicus can model both impulsive and finite thrust maneuvers, as well as perform constrained optimization. Trajectories are modeled as segments, with impulsive maneuvers possible at the beginning and end of each segment, and finite thrust possible throughout each segment. Successive segments can inherit the values of parameters from previous segments, or they can be

independent. In fact, successively numbered segments are not even required to model the same orbit or spacecraft. These features make Copernicus a very flexible trajectory modeling and optimization package. The only gravitating bodies included in this analysis were the sun and the earth, although Copernicus has the capability of including a large number of bodies in the model.

Table 13: WBS and mass properties for the solar collector mitigation option

WBS Element - Solar Collector			Qty	Unit Mass (kg)	Total Mass (kg)
	Primary Collector				**233**
		Membrane	1	63	63
		Inflatable Struts	1	140	140
		Inflation Mechanism	1	30	30
	Secondary Collector				**573**
		Collector	1	211	211
		Collector Struts	1	63	63
		Thermal	1	154	154
		Avionics	1	14	14
		Power	1	131	131
	Tip Vanes				**348**
		Structure	4	15	60
		Thermal	4	5	20
		Avionics	4	55	220
		Power	4	12	48
	Growth				**346**
		Primary Colector	30%	-	70
		Secondary Collector	30%	-	172
		Tip Vanes	30%	-	104
Dry Mass					**1500**
	Non-Cargo				**0**
	Cargo/Payload				**0**
Inert Mass					**0**
	Non-Prop Fluids				**0**
Total Less Propellant					**1500**
	Propellant				**0**
Gross Mass					**1500**

The planetary body named Apophis is anticipated to pass well within the moon's orbit in April of 2029. Given this fact, the authors decided to make Apophis the subject of the deflection analysis. But before beginning, just as in the previous study,[2] the analysts had to modify the orbital elements of Apophis to force it to collide with the earth on or around April 2029. These calculations were done by Copernicus. The actual ephemeris data for Apophis came from the JPL Horizons ftp server (horizons.jpl.nasa.gov) and was entered into Copernicus. Then several orbital elements were varied until the planetary body collided with Earth, dead center.

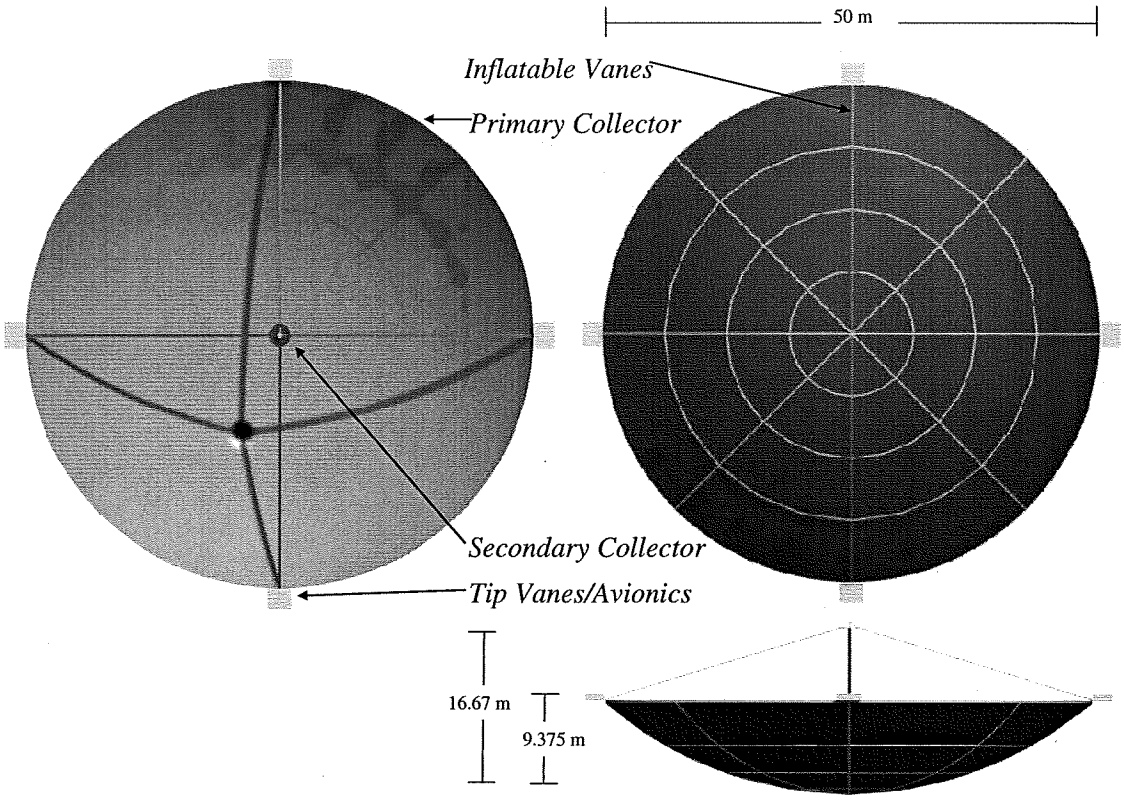

Figure 15: Major components and dimensions of the solar collector system

Table 14. Orbital elements for Apophis and the modified orbital elements for the fictitious asteroid M-Apophis. The modified elements result in a collision with Earth on the date shown.

Source	JPL Horizons ftp server
Epoch	2029 January 01, 0 hms (2462137.5)
Collision date	2029 April 22, 12:10:10.73
System	Heliocentric, ecliptic of J2000

	Original	Modified
SMA	137986931.808626	137978976.282590
ecc	0.19114698829234	0.19091399221024
inc	3.34145210222811	3.33334821309700
RAAN	203.87408043057400	212.35750466471000
AOP	126.69571964824600	127.46966492194000

From these values the authors calculated the state vector for M-Apophis on the collision date. The state vector for Earth and M-Apophis were then entered into PBI, which determined the impulsive delta-v values required to successfully deflect the asteroid. The number of days before impact, which represents the time at which the impulsive delta-v takes place, was allowed to vary in 50 day increments from 50 days before Earth impact to 3000 days before Earth impact. As a check, a few cases were also completed using Copernicus, and the results were nearly identical. PBI was used, however, because it can compute the delta-v's for all the impulsive cases in a single run.

Figure 16 below shows the required impulsive delta-v values required to successfully deflect M-Apophis. Since the nuclear blast and the kinetic interceptor options are modeled as impulsive events, Figure 16 shows the delta-v values required from these two deflection mechanisms. As expected, the delta-

v requirements are very large if the asteroid is only a few months away from collision. However, if intercepted far enough in advance, the required delta-v can be as low as approximately 5 cm/s.

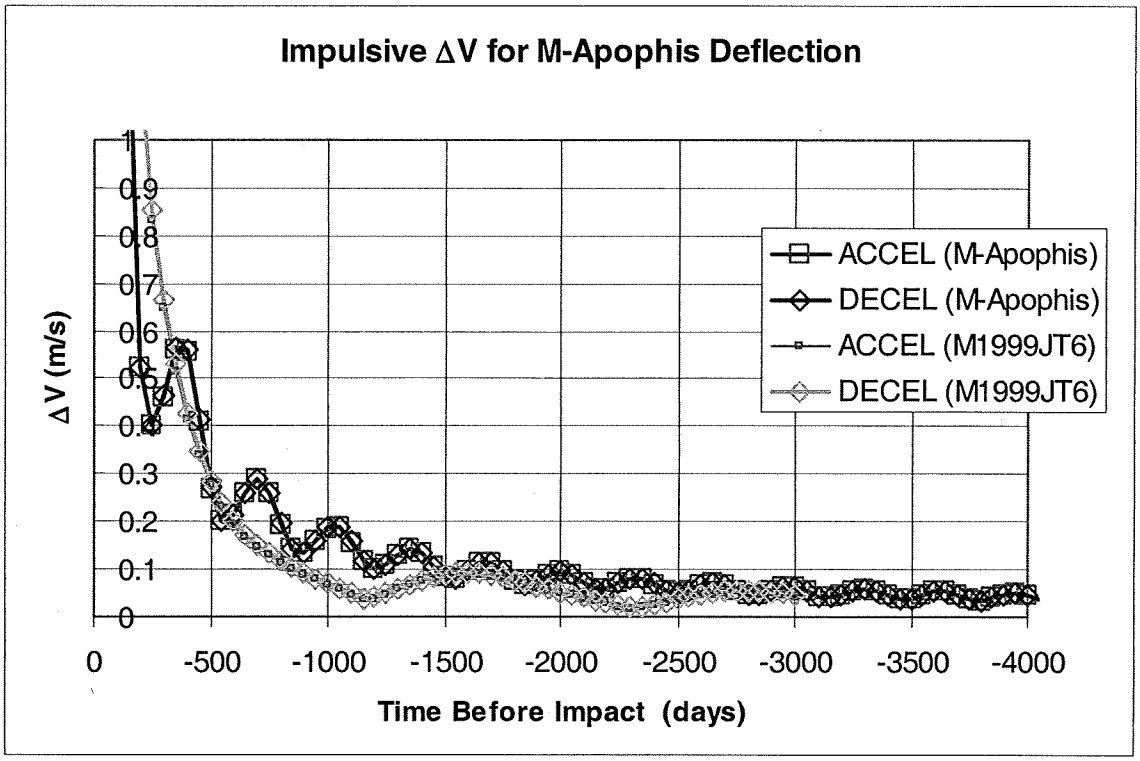

Figure 16. Impulsive delta-v required to successfully deflect the fictitious asteroid M-Apophis and cause it to miss Earth's surface by 3 Earth radii. Note that there is virtually no difference in the delta-v requirements for accelerating or decelerating the asteroid.

While applying the impulsive manuever 500 days or more before impact appears to lower the delta-v requirement, the cyclic component of the graph suggests that applying the delta-v at certain points in M-Apophis's orbit may be more advantageous. When one looks at the position of M-Apophis at the peaks and valleys on the plot, one will see that the valleys correspond to the times when the planetary body is near perihelion, and the peaks correspond to the times when the planetary body is near apohelion.

The finite thrust analysis, which corresponds to the solar collector deflection option, was analyzed using Copernicus. And while Copernicus can model the thrust in any direction, the authors decided to initially limit the thrusting to be parallel with the velocity vector of the asteroid, causing either acceleration or deceleration, and then allow Copernicus to optimize the thrusting direction for a few cases in order to compare the benefits of unconstrained thrust angles. The authors selected 1,000,000 kg as the mass of the asteroid; this data was entered into Copernicus, as well as the number of days before Earth impact when the solar collector began working. With this information, Copernicus was allowed to determine the initial thrust required to successfully deflect the asteroid. The solar collector option was modeled as a solar electric propulsion system so that the effect of the distance from the sun would be included. Given the mass of the asteroid and the force required, the authors could determine the acceleration required to deflect the asteroid.

The deflection requirements are shown in Figure 17. Once again, there is little difference between accelerating and decelerating the asteroid, but clearly the length of time that the solar collector can act greatly influences the required acceleration. A rendezvous at 600 days before impact, and with continuous operation of the solar collector, requires an acceleration of 9.4×10^{-9} m/s^2, which results in a thrust of 0.0094 N for our baseline one million kilogram asteroid. These values drop by an order of magnitude if the rendezvous occurs around 2000 days before Earth impact.

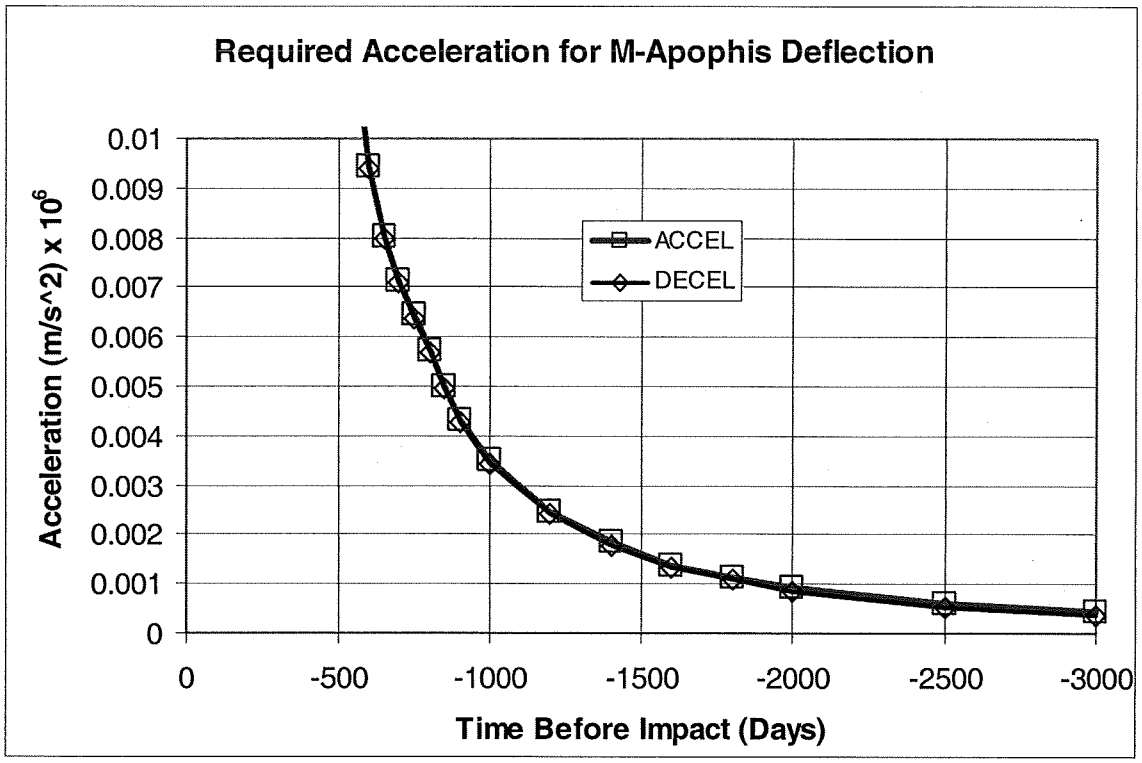

Figure 17. Acceleration required to successfully deflect the fictitious asteroid M-Apophis versus the number of days before impact at which the deflection mechanism begins operating. As with the impulsive option, there is little difference between the accelerating and decelerating cases, although decelerating has a slight advantage if the operating time is greater than about 1500 days.

The kinetic deflection option resulted in the most complex trajectory models. The team assumed that the impulse applied by the kinetic interceptor would not be parallel to the velocity vector of M-Apophis, which means that the impulsive ΔV values from the ACCEL and DECEL maneuvers would not be applicable. The approach was to allow Copernicus, given the number of days before Earth impact at which the kinetic interceptor is to collide with M-Apophis, to determine the trajectory which resulted in the maximum encounter velocity relative to M-Apophis. In fact, the ΔV required to rendezvous with M-Apophis was actually determined, which maximized the relative encounter velocity. The TAI ΔV was constrained to a maximum of 8590 m/s, and the rendezvous ΔV to a maximum of 10000 m/s (due to limits of the targeting system). Given that the opposite direction of the rendezvous ΔV vector is the direction of the momentum exchange when the kinetic interceptor collides with the target, PBI was given that vector and used to determine the minimum ΔV in that direction that would successfully deflect the planetary body.

The results are listed in Table 15. Since the outbound and inbound analysis of the kinetic interceptor could not be decoupled (unlike the other deflection options), and the analysis was more complicated, only a portion of the trajectory trade space could be analyzed. However, the results shown in the table do provide insight into the kinetic deflection requirements. The kinetic interceptor does not generally impart an impulse in a direction parallel to the planetary body's velocity vector, meaning that the results shown in Figure 16 could not be used. Instead, the ΔV magnitude is the impulse required along the delta-velocity vector at collision, and does not necessarily agree with the values in Figure 16. The first column in the table is the time before Earth impact (TBI) at which the interceptor collides with the planetary body. The second column lists the number of days before Earth impact at which the interceptor departs from LEO. The far right three columns show the ΔV required to travel to M-Apophis, the relative velocity of the impact, and the required ΔV that the interceptor must deliver for a successful deflection, respectively. In most of the cases for which Copernicus could find a solution, either the TAI ΔV or the encounter relative velocity were at a maximum. The reason is that the encounter relative velocity was always maximized, but constrained, and the launch vehicle and departure stages provide plenty of ΔV for reaching Apophis. Given

the required ΔV in the last column, the mass of the asteroid, and the relative encounter velocity, one can determine the required mass of the kinetic interceptor. Clearly, intercepting the asteroid 2000 to 2500 days before Earth impact requires a significantly smaller kinetic interceptor mass.

Table 15. Launch and Encounter Data for M-Apophis Using the Kinetic Interceptor Option. Knowing the required ΔV (final column), the encounter relative velocity (5th column), and the asteroid mass, one can determine the required kinetic impactor mass.

TBI at Intercept (days) Intercept	TBI at TAI (days) Launch	Trip Time (days)	TAI DV (km/s)	Encounter (km/s)	Req. DV (m/s)
-50	-124.07	74.07	4.44	10.00	6.9312
-100	-176.07	76.07	6.82	10.00	1.8303
-150	-209.54	59.54	8.59	8.11	1.0094
-200	-297.38	97.38	3.55	10.00	5.4441
-250	-387.80	137.80	6.46	10.00	0.6762
-300	-422.09	122.09	8.59	8.34	0.4054
-350	-454.32	104.32	8.59	6.47	0.4199
-400	-475.70	75.70	8.59	7.38	0.7608
-450	-529.49	79.49	5.69	10.00	0.4262
-650	-858.36	208.36	8.59	6.85	0.1588
-700	-883.34	183.34	8.59	8.66	0.1841
-750	-958.47	208.47	5.91	10.00	1.2039
-2000	-2164.53	164.53	8.59	9.08	0.0826
-2100	-2299.94	199.94	4.96	5.68	0.0518
-2500	-2740.21	240.21	6.15	10.00	0.0422

One should note, however, that maximizing the relative encounter velocity does not necessarily result in the smallest interceptor mass. In the table, the direction of the impulse imparted on the asteroid is not in an optimal direction, and it is possible that a different outbound trajectory with a lower relative velocity could result in a lower required ΔV for deflection *and* a lower interceptor mass. However, time constraints prevented the study team from searching for global optimum values since two separate trajectory tools were required to complete the kinetic interceptor trajectory analysis.

Unlike the kinetic deflection option, the impulse imparted on the asteroid by the nuclear blast can be made parallel to the planetary body's velocity vector, so the inbound ΔV requirements can be read from Figure 16. For the outbound trajectory, which was analyzed using Copernicus, the velocity of the nuclear mechanism relative to the asteroid was minimized while constraining the TAI ΔV to be less than 8590 m/s. The results are listed in Table 16. For the outbound trajectory, no real benefits result from launching the deflection mechanism at earlier dates. This is the opposite of the inbound trajectories, where acting on the asteroid far in advance greatly reduces the ΔV requirements.

Table 16. Outbound Trajectory Results for the Nuclear Deflection Option.

TBI at Encounter (days)	TBI at TAI (days)	Trip Time (days)	TAI DV (km/s)	Encounter Relative Velocity (km/s)
-150	-254.14	104.14	4.80	3.72
-200	-365.12	165.12	3.80	7.66
-250	-410.83	160.83	6.09	7.78
-300	-466.45	166.45	6.18	3.88
-350	-644.98	294.98	3.29	3.36
-550	-867.92	317.92	8.10	2.05
-600	-897.81	297.81	7.41	1.94
-650	-909.50	259.50	8.27	3.19
-700	-932.32	232.32	6.15	5.87
-750	-967.82	217.82	6.53	9.82
-800	-1199.58	399.58	8.30	5.64
-850	-1226.38	376.38	7.28	2.79
-900	-1256.93	356.93	7.20	2.42
-950	-1296.84	346.84	6.25	3.26
-1000	-1287.67	287.67	8.12	7.03
-1200	-1610.98	410.98	8.55	2.94
-1500	-1963.48	463.48	8.42	3.66
-2000	-2208.16	208.16	7.63	3.68

IX. Comparison of Interceptor Capabilities

The previous two sections illustrate the capabilities of the three considered mitigation options to impart a ΔV or acceleration to an incoming NEO, and the required ΔV or acceleration to cause an NEO to miss Earth as a function of time before impact. At this point it makes sense to combine the results of the two sections and compare results. The next three figures illustrate the combined performance/requirement of each of the three concepts. Figure 18 represents the capability of the nuclear interceptor option. To read this chart one needs to imagine a vertical line through some portion of the chart. Where the line crosses will determine the time required and NEO size that can be deflected. For instance imagine a vertical line through a ΔV of 0.4 m/s. That line would cross the NEO diameter at about 400 m. Also it would cross the time before impact line at about 300 days. Thus the nuclear interceptor option can deflect an NEO of up to 400 m with 300 days warning. In fact careful consideration of Figure 18 suggests that the nuclear interceptor can deflect NEO's up to 500 m with about 2 years warning and larger NEO's with 5-10 years warning.

Figure 19 is a similar illustration of the kinetic interceptor option. This chart shows that the kinetic interceptor is not able to produce sufficient DV to deflect any but the smallest (0-100 m) NEO's. However recalling that the cradle can carry up to 6 of these missiles, the figure also shows the combined performance of all 6 kinetic interceptors. Here, given 8-10 years warning, the kinetic interceptor may be able to deflect NEO's of 300-400 m.

Figure 20 shows the combined effects for the solar collector. Here the x-axis is the net acceleration imposed by the solar collector. Assuming that acceleration is imposed from time before impact continuously until the NEO reaches Earth, the figure shows the minimum acceleration needed to miss the Earth by 3 Earth radii. The solar collector looks effective for all sizes of NEO's up to 1 km albeit with increasing operation times with increasing NEO diameter. At the larger diameters, the solar collector can require 10 years of operation, which would be difficult to do in practice. However recalling that the cradle can carry 6 solar collectors, it is possible to swap out collectors as they degrade to maintain continuous acceleration. Although not considered here, it is probable that the acceleration near Earth is not as effective as the initial acceleration, and that the operation times are not as long as depicted here.

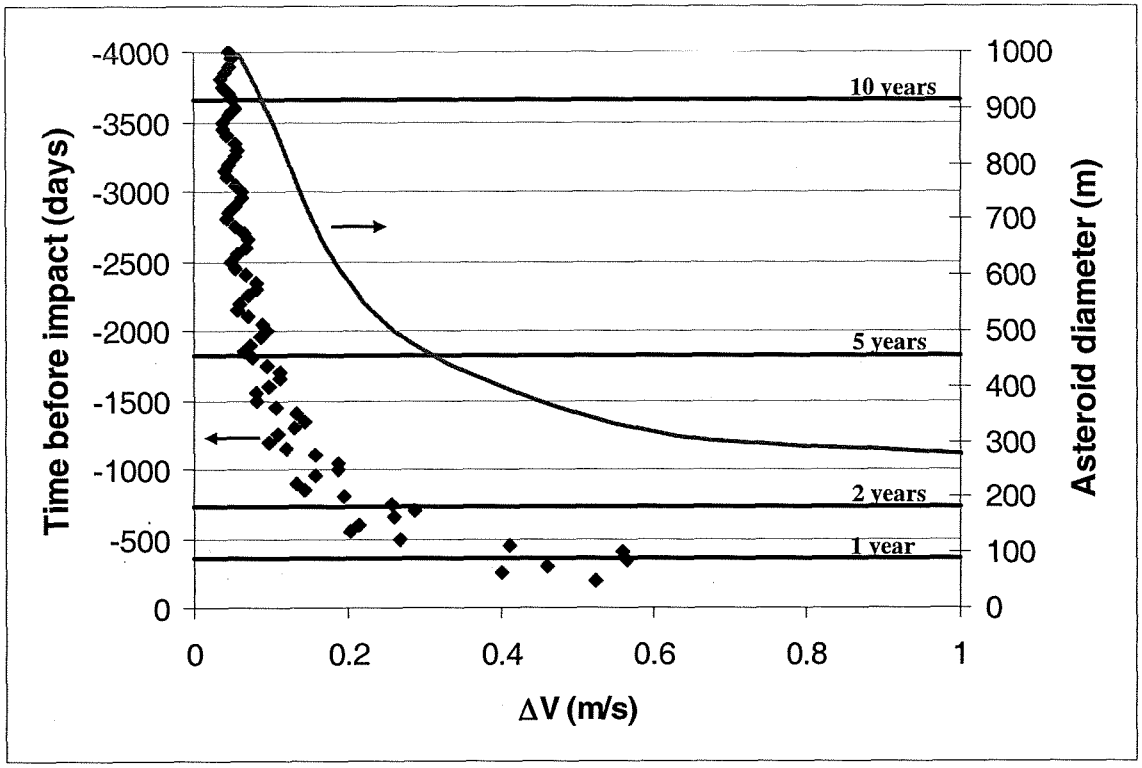

Figure 18: Comparison of nuclear interceptor effectiveness and time before impact as a function of ΔV

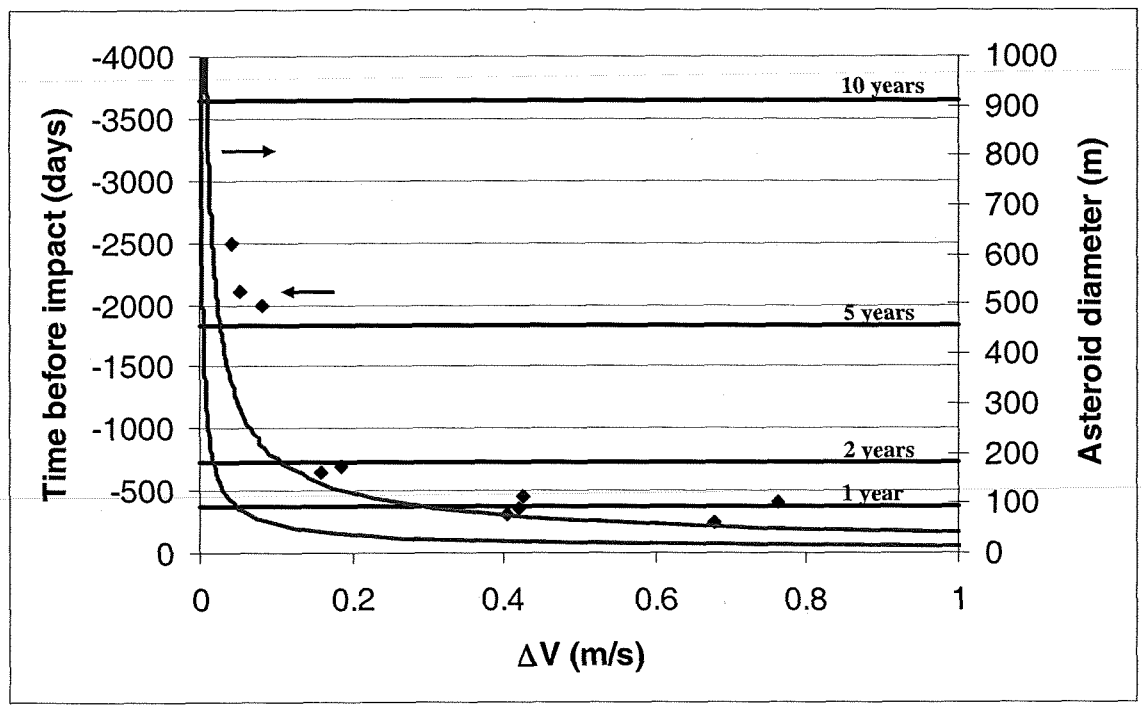

Figure 19: Comparison of kinetic interceptor effectiveness and time before impact as a function of ΔV

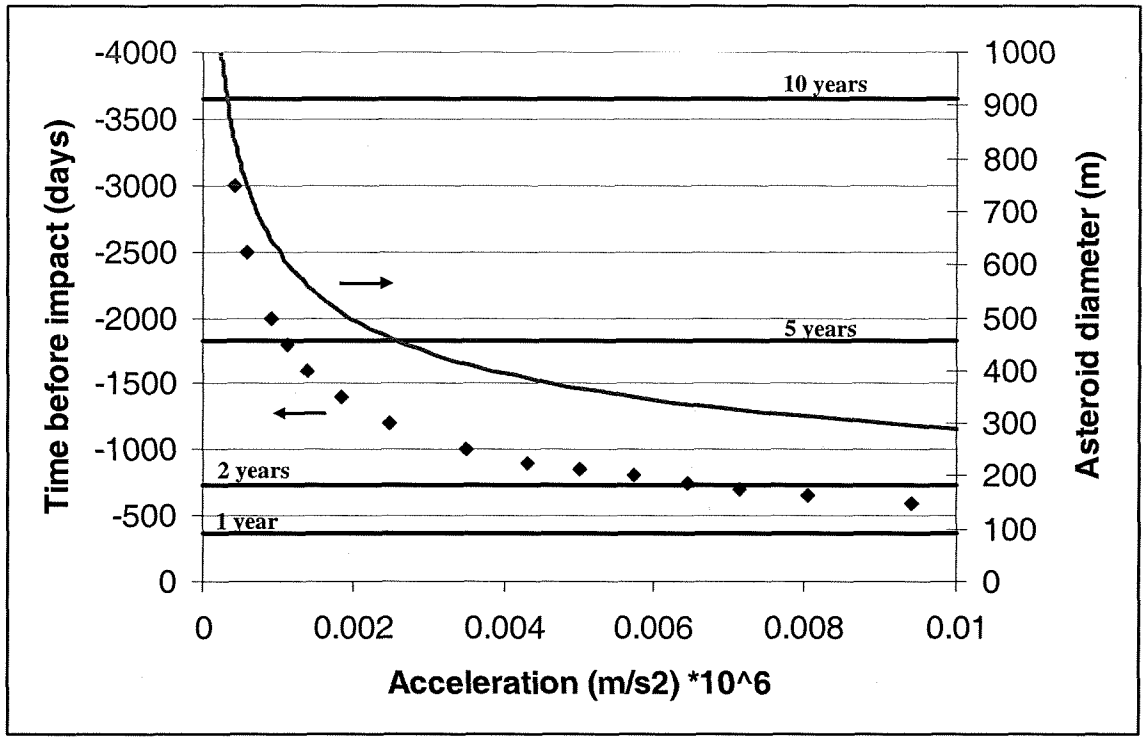

Figure 20: Comparison of solar collector effectiveness and time before impact as a function of acceleration.

X. Conclusions

In conclusion it is evident that the nuclear interceptor option can deflect NEO's of smaller size (100-500 m) with 2 years or more time before impact, and larger NEO's with 5+ years warning. The kinetic interceptors may be effective for deflection of NEO's up to 300-400 m diameter but require 8-10 years warning time. Solar collectors show promise for deflection of NEO's if issues pertaining to long operation time can be overcome. And finally the Ares I and Ares V vehicles show sufficient performance to enable development of a near term categorization and mitigation architecture.

XI. Open Issues

The efforts described herein are the result of a short term intense study. There are many issues the authors would like to address in a more detailed long term design effort. The architecture has several issues outstanding, as does the design and modeling of each interceptor option.

For the architecture there are several issues to be addressed. First more detailed designs for all vehicles are indicated to drive out all issues not uncovered in out preliminary design. The interceptor stage was almost double the size of the observer TAI stage which suggests possible reuse of Lox/LH2 stage in both observer and interceptor stacks. Finally the TAI stage was of similar mass to the existing Centaur stage which suggests possible use of an existing stage.

For the nuclear interceptor option there are details to be worked out in the design and modeling of the nuclear explosion and its interaction with the NEO. Future efforts should include neutron flux in asteroid deflection models. There is still significant uncertainty in asteroid composition, which should be addressed in the interaction model between the resultant neutron and x-ray spectrum and the asteroid composition. The authors would like to continue research into existing terminal guidance technologies under development for missile defense systems. And more investigation of the optimal stand off distance and the ability to respond accurately enough to explode at the optimal stand off point should be addressed.

For the kinetic interceptor the authors were not able to include the design of the solar electric propulsion system effects in shaping the interceptor orbit to strike at the optimal velocity and impact direction. Modeling of the penetrator interaction with the asteroid is indicated. For the solar collector the authors wish to expand their investigation of the issues surrounding heating of secondary collector. Reaching a

lower rejection temperature would enable higher TRL heat pipe technology. Estimates of beam divergence and focusing require refinement.

Finally the authors would like to demonstrate possible other uses for the proposed planetary defense architecture. Utilization of resources on these NEO's could enable or enhance future human and robotic missions. Additionally the proposed architecture could be used to support human/robotic missions to NEO's, Mars, and beyond.

Acknowledgments

The authors wish to express their appreciation to the MSFC New Business office for the funding to complete this follow on study. This work would not have been possible without this MSFC internal funding, and the willingness of the administrators of these funds, Dr. John Horack and Dr. Les Johnson, to consider the need to continue this research.

Additionally the authors would like to recognize the efforts of the authors of the original NASA-TP. Those authors, Reginald Alexander, Dr. Joseph Bonometti, Jack Chapman, Sharon Fincher, Randy Hopkins, Matt Kalkstein, and Tara Polsgrove of NASA- MSFC, as well as Dr. Geoff Statham and Slade White of ERC, Inc. were a pleasure to work with on this project. Much of the results in this current study would not have been possible without their considerable and well documented efforts and their willingness to share their knowledge in support of this effort.

References

[1] "The Vision for Space Exploration", NP-2004-01-334-HQ, Washington, DC, February 2004.

[2] Adams, R. B., Alexander, R. Bonometti, J., Chapman, J., Fincher, S., Hopkins, R. Kalkstein, M., Polsgrove, T., Statham, G., White, S.,, *Survey of Technologies Relevant to Defense from Near-Earth Objects*, NASA-TP-2004-213089, NASA-MSFC, July 2004.

[3] Barrera, Mark J., "Conceptual Design of an Asteroid Interception for A Nuclear Deflection Mission,"2004 Planetary Defense Conference: Protecting Earth from Asteroids, Orange County, February 2004.

[4] Regeon, P. and Chapman, R.J., "Clementine Lunar Orbiter Spacecraft System Design," AAS-95-130, 1995.

[5] Hughes, Michael P., and Schira, Charles N., "Deep Impact Attitude Estimator Design and Flight Performance," American Astronautical Society, G & C Conference, Breckenridge, CO, February 4, 2006.